Choosing Public Datasets for Private Machine Learning via Gradient Subspace Distance

Anonymous authors
Paper under double-blind review

Abstract

Differentially private stochastic gradient descent privatizes model training by injecting noise into each iteration, where the noise magnitude increases with the number of model parameters. Recent works suggest that we can reduce the noise by leveraging public data for private machine learning, by projecting gradients onto a subspace prescribed by the public data. However, given a choice of public datasets, it is unclear why certain datasets perform better than others for a particular private task, or how to identify the best one. We provide a simple metric which measures a low-dimensional subspace distance between gradients of the public and private examples. We empirically demonstrate that it is well-correlated with resulting model utility when using the public and private dataset pair (i.e., trained model accuracy is monotone in the distance), and thus can be used to select an appropriate public dataset. We provide theoretical analysis demonstrating that the excess risk scales with this subspace distance. This distance is easy to compute and robust to modifications in the setting.

1 Introduction

Recent work has shown that machine learning (ML) models tend to memorize components of their training data (Fredrikson et al., 2015), and in fact attackers can often recover training samples from published models through carefully designed attacks (Carlini et al., 2021; Shokri et al., 2017). This is a critical privacy issue when models are trained on private data. A popular approach to address this issue is to adopt *Differential Privacy* (DP) (Dwork et al., 2006) as a rigorous privacy criterion that provably limits the amount of information attackers can infer about any single training point. *Differentially private stochastic gradient descent* (DPSGD) (Abadi et al., 2016; Song et al., 2013; Bassily et al., 2014) is one of the most commonly used methods to train a ML model (differentially) privately. It makes two main modifications to vanilla SGD: 1) clipping per-sample gradients to ensure a bound on their ℓ_2 norms; 2) adding Gaussian noise to the gradient.

One downside of adopting DP in ML is that we need to sacrifice utility of the trained model to guarantee privacy. Specifically, DPSGD noises the gradient at each step, with noise drawn from a spherical Gaussian distribution, $\mathcal{N}\left(\mathbf{0}, \sigma^2 \boldsymbol{I}_p\right)$, where p is the model dimension (i.e., the number of model parameters) and the variance σ^2 scales the noise. In order to bound the privacy leakage, the magnitude of noise introduced in each step must scale with the square root of the number of parameters p. Consequently, for many large models, the noise introduced may overwhelm the signal contributed by the original gradients, significantly diminishing the utility.

Several works have proposed methods to improve the utility of private machine learning (Zhou et al., 2021; Golatkar et al., 2022; Luo et al., 2021; Yu et al., 2021; Kairouz et al., 2021; Nasr et al., 2023; Ganesh et al., 2023; Lee & Kifer, 2018). One fruitful direction uses *public* data, i.e., data that is not subject to any privacy constraint. There are primarily two types of approaches that incorporate public data in private training. The first involves *transfer learning*, where we pretrain the model on a public dataset and then (privately) finetune the model on a sensitive dataset for our target task (Luo et al., 2021; Abadi et al., 2016; Yu et al., 2022; Li et al., 2022c). Another approach is based on *pre-conditioning*, which exploits the empirical observation that during training, the stochastic gradients (approximately) stay in a lower-dimensional subspace of the p-dimensional gradient space. Consequently, some works find this subspace using the public data, and then

project the sensitive gradients to this (public) subspace before privatization (Zhou et al., 2021; Golatkar et al., 2022; Yu et al., 2021; Kairouz et al., 2021). This reduces the magnitude of the introduced noise and generally improves utility over DPSGD without supplementary data.

However, this raises a number of natural questions. From a scientific perspective: why do some public datasets work better than others for a particular private task? One may intuitively believe that public datasets which "look relevant" to the private task would perform best, but this is not a precise statement, and furthermore (as we will empirically demonstrate) may be misleading or incorrect. Building on this question, from a pragmatic standpoint, how should one select which public dataset to use?

Our main contribution addresses both of these questions: we provide a simple metric for measuring the distance between datasets, and show that it is very well-correlated with model utility when treating one dataset as private and the other as public.

Table 1: GEP evaluation AUC and corresponding distance in descending order. We use the *same* model setting for private training and distance computation. "-" means DP-SGD training without using any public data. We use $\epsilon = 2, \delta = 1e-5$. Mean and standard deviation are calculated over 3 runs.

AUC	Private Dataset	Public Dataset	Distance
68.93% / 0.05	ChestX-ray14	ChestX-ray14	**0.15**
67.22% / 0.21		SprXRay	0.32
67.20% / 0.34		CheXpert	0.32
66.61% / 0.04		KagChest	0.36
65.37% / 0.43		Kneeos	0.38
64.76% / 0.16		-	-
48.60% / 0.02		CIFAR-100	0.55
Time cost for each distance computation: **12s**			

We demonstrate its efficacy in both transfer learning and pre-conditioning settings. To summarize our contributions:

1. **We introduce Gradient Subspace Distance (GSD), a metric to quantify the difference between private and public datasets.** GSD is an easily computable quantity that measures the distance between two datasets.

2. **We find GSD is well-correlated with model utility when selecting public datasets in both pre-conditioning and transfer learning settings.** As a representative example, Table 1 shows the utility of a privately trained model using a public dataset increases monotonically as GSD decreases. Our theoretical analysis demonstrates that the excess risk of Gradient Embedding Perturbation (GEP) (a private training algorithm that leverages public data for gradient pre-conditioning) scales with the GSD.

3. **We show that GSD is *transferable*.** The ordering of GSD for several choices of public dataset remains fixed across architectures, both simple (e.g., 2-layer CNN) and complex. Using these simple architectures as a proxy, we can efficiently compute GSDs which are still useful for privately training large models.

2 Related Work

Transfer Learning. In the differentially private setting, it is now common to pre-train a model on public data, and then privately fine-tune on private data. This can result in comparable utility as in the non-private setting, evidenced for both language models (Yu et al., 2021; 2022; Li et al., 2022c) and vision tasks (Luo et al., 2021; De et al., 2022; Mehta et al., 2022). In many cases, due to computational requirements, it may be challenging to pre-train a large model on a public dataset. Instead, many practitioners will turn to pre-trained weights, which obviate the computational burden, but give less flexibility to choose an appropriate training

dataset. As a result, we use second-phase pre-training, in which we perform a second phase of pre-training with a modestly-sized public dataset. This has been proven to be useful in non-private setting (Gururangan et al., 2020).

Pre-conditioning. Empirical evidence and theoretical analysis indicate that while training deep learning models, gradients tend to live in a lower-dimensional subspace (Gur-Ari et al., 2018; Li et al., 2020; 2022b; Golatkar et al., 2022; Kairouz et al., 2020). This has led to methods for private ML which project the sensitive gradients onto a subspace estimated from the public gradients. By using a small amount of i.i.d. public data, Zhou et al. (2021) demonstrate that this approach can improve the accuracy of differentially private stochastic gradient descent in high-privacy regimes and achieve a dimension-independent error rate. Similarly, Yu et al. (2021) proposed GEP, a method that utilizes public data to identify the most useful information carried by gradients, and then splits and clips them separately. Amid et al. (2022) proposed a DP variant of mirror descent that leverages public data to implicitly learn the geometry of the private gradients. In the first-order approximation, it can be considered as using public gradients as a regularizer for DP-SGD. Gradient estimation based on public data can also be used as a preconditioner for adaptive optimizers like RMS-Prop (Li et al., 2022a).

Domain Adaptation. We aim to quantify the similarity between private and public datasets. One related area of research is distribution shift, or domain adaptation (Gabrel et al., 2014; Wang & Deng, 2018; Zhuang et al., 2019; Zhang, 2019; Ben-David et al., 2010; 2006; Wang et al., 2021). At a high level, research in this area examines the problem of when the distributions of test and training data differ, which aligns with our goals. However, most work in this area focuses on reducing the gap between in- and out-of-distribution test errors, where target data is used repeatedly for accuracy improvement. Most of the work along this line assumes that the target data is also public or doesn't consider privacy, and is thus inappropriate for the private learning setting. To the best of our knowledge, the only work with a similar focus to us is Task2Vec (Achille et al., 2019), which uses the Fisher information matrix to represent a dataset as a vector, allowing for the measurement of a distance between two datasets. However, it is not suitable for private learning tasks as our empirical evaluation shows that Task2Vec fails to accurately rank the utility of public datasets.

Choosing Proper Public Data For Private ML. Perhaps the most comparable work is the independent and concurrent work of Yu et al. (2023), as both aim to select the best public data for private machine learning. Yu et al. (2023) propose a private learning framework that uses private dataset selection to choose a subset of the pre-training dataset. While our goals are similar, there are differences in our methods and use cases. Our work focuses on scenarios with limited amounts of public data. In contrast, Yu et al. (2023) focuses on first-phase pretraining with large-scale datasets (see Figure 2). However, this is only applicable for organizations with large computational resources, who can afford to pretrain such large models. In contrast, we believe most practitioners and researchers (ourselves included) are much more compute-constrained, and will rely upon already pre-trained models, with little control over the first-phase pretraining set. This is the focus of our work. Finally, their method requires training a full-sized DP model, whereas our method can be executed in less than a minute.

3 Preliminaries

Notation. We use $\mathcal{Z}$ to represent dataspace. We use $\Theta \in \mathbb{R}^p$ to denote parameter space, p is the model dimension, i.e., the number of parameters in the model, k is a parameter we will use to denote the dimension of the lower-dimensional space we choose. m refers to the number of examples in a batch. We use superscripts and subscripts interchangeably to denote private or public data, like x_{priv}, V^{pub}.

Definition 1 (Differential Privacy (Dwork et al., 2006)). *A randomized algorithm $\mathcal{A}$ is* (ϵ, δ)-differential private *if for any pair of datasets D, D' that differ in exactly one data point and for all subsets $\mathbb{S}$ of outputs, we have:*

$$\Pr[\mathcal{A}(D) \in \mathbb{S}] \leq e^{\epsilon} \Pr[\mathcal{A}(D') \in \mathbb{S}] + \delta.$$

Definition 2 (Principal Angles (Golub & Loan, 1996)). *Let V_1 and V_2 be two orthonormal matrices of $\mathbb{R}^{p\times k}$. The* principal angles $0 \leq \theta_1 \leq \cdots \leq \theta_k \leq \pi/2$ *between two subspaces span(V_1) and span(V_2), are defined recursively by*

$$\cos\theta_k = \max_{\mathbf{u_k}\in span(V_1)} \max_{\mathbf{v_k}\in span(V_2)} \mathbf{u_k'}\mathbf{v_k}, \quad \textit{subject to}$$

$$\mathbf{u_k'}\mathbf{u_k} = 1, \mathbf{v_k'}\mathbf{v_k} = 1, \mathbf{u_k'}\mathbf{u_i} = 0, \mathbf{v_k'}\mathbf{v_i} = 0, i = 1, ..., k-1$$

That is, the first principal angle θ_1 is the smallest angle between all pairs of unit vectors over two subspaces, the second θ_2 is the second smallest angle, and the rest are similarly defined.

Definition 3 (Projection Metric (Ham & Lee, 2008; Edelman et al., 1998)). *The* projection metric *between two k-dimensional subspaces V_1, V_2 is defined as:*

$$d\left(V_1, V_2\right) = \left(\sum_{i=1}^{k} \sin^2\theta_i\right)^{1/2} = \left(k - \sum_{i=1}^{k} \cos^2\theta_i\right)^{1/2}$$

where the θ_i's are the principal angles between V_1 and V_2.

Gradient Embedding Perturbation (GEP). Our theoretical analysis is based on GEP (Yu et al., 2021), a private learning algorithm that leverages public data for gradient preconditioning. We note that GEP is the leading approach among private ML algorithms that use public data for preconditioning, and produces state-of-the-art results. Hence, for preconditioning-based methods, we focus entirely on GEP. Here we briefly introduce their algorithm. GEP involves three steps: 1) it computes a set of the orthonormal basis for the lower-dimensional subspace; 2) GEP projects the private gradients to the subspace derived from step 1, thus dividing the private gradients into two parts: embedding gradients that contain most of the information carried by the gradient, and the remainder are called residual gradients; 3) GEP clips two parts of the gradients separately and perturbs them to achieve differential privacy. The full algorithm is in Appendix A.

4 Gradient Subspace Distance

Let's consider a private supervised learning task on private dataset $D^{priv} \in \mathcal{Z}^n_{priv}$, with a differentially private learning algorithm A that can leverage public data to improve model utility. We have a collection of potential choices of public datasets $[D^{pub}_1 \in \mathcal{Z}^{n1}_1, D^{pub}_2 \in \mathcal{Z}^{n2}_2, \cdots]$. We would like a metric that, when computed for a public dataset D^{pub}, is well-correlated with utility when D^{pub} is used as the public dataset with algorithm A on private task D^{priv}. This serves two purposes: first, it gives a quantitative metric that can formalize dataset similarity and suitability for use as a public dataset. Second, it may be useful in actually *selecting* a public dataset for use for a particular private task, which is a critical hyperparameter.

Algorithm 1 Gradient Subspace Distance (GSD)

Input: A batch of private samples from D^{priv}: $x_{priv} \in \mathcal{Z}^m_{priv}$, a batch of private samples public examples from D^{pub}: $x_{pub} \in \mathcal{Z}^m_{pub}$, model weights $\mathbf{w}_0 \subset \Theta$, loss function $\mathcal{L} : \Theta \times \mathcal{Z} \to \mathbb{R}$, dimension k
Output: Distance between two image datasets $\boldsymbol{d}$

1: `// Compute per-sample gradient matrix for private and public examples`
2: $G_{priv} = \nabla\mathcal{L}(\mathbf{w}_0, x_{priv})$
3: $G_{pub} = \nabla\mathcal{L}(\mathbf{w}_0, x_{pub})$
4: `// Compute top-`k` subspace of the gradient matrix`
5: $U^{priv}, S^{priv}, V^{priv} \leftarrow \mathbf{SVD}(G_{priv})$
6: $U^{pub}, S^{pub}, V^{pub} \leftarrow \mathbf{SVD}(G_{pub})$
7: `// Compute the distance between two subspaces`
8: $\boldsymbol{d} = \mathbf{ProjectionMetric}(V^{priv}_k, V^{pub}_k)$

We present the pseudo-code of our algorithm, Gradient Subspace Distance (GSD) in Algorithm 1. At a high level, our method involves the following two steps: finding the gradient subspace of the public and

private data examples, and computing their gradient subspace distance. The algorithm uses the same model A and a batch of randomly labeled data examples from private and public datasets. Following standard DP-SGD, the algorithm will first compute and store per-example gradients from each data example, that is $G_{priv}, G_{pub} \in \mathbb{R}^{m \times p}$. Then it computes the top-k singular vectors of both the private and public gradient matrix by performing singular value decomposition (SVD). Finally we use projection metric to derive the subspace distance $\boldsymbol{d}$ by taking the right singular vectors V_k^{pub}, V_k^{priv} from the previous step.

GSD is naturally suited to the aforementioned pre-conditioning methods. In each iteration, these methods project the private gradients to a low-dimensional subspace, which ideally contains most of the signal of the gradients[1]. Since repeatedly selecting the top subspace of the gradients themselves is not a privacy-preserving operation, we instead choose a public dataset to use as a proxy. Thus intuitively, a public dataset with a "similar top subspace" should be suitable. This is what GSD tries to capture, and the best dataset should be the one with minimum GSD.

However, following this intuition only gets us so far: taking it literally would measure distances between the public and private datasets at each step throughout the training process, an impractical procedure that would introduce significant overhead. Remarkably, we instead find that a simple alternative is effective: compute the distance only once at initialization (Section 4.2). This requires only a single minibatch of each dataset, and as we show in our experiments, is surprisingly robust to changes in model architecture (Section 6.3). Most importantly, we show that it is also effective for *transfer learning* settings (Section 6.2), where subspace projections are not used at all, thus demonstrating that GSD more generally captures dataset similarity and fitness-for-use of public datasets.

4.1 Excess Risk Scales with GSD

In this section, we theoretically prove that the excess risk of a pre-conditioning public-data-assist private machine learning algorithm, e.g., GEP (Yu et al., 2021), is bounded by Gradient Subspace Distance (GSD) under standard statistical learning assumptions. We first show that the reconstruction error $\|\mathbf{G}_{priv} - \mathbf{G}_{priv} V^{pub} V^{pub\top}\|_2$ is bounded by GSD. Then we show that the convergence bound of excess risk is determined by the reconstruction error.

Lemma 4.1 (**Reconstruction Error**). *For GEP, let $\mathbf{G}_{priv}$, V^{pub}, V^{priv} be the gradient matrix and top-1 gradient subspace from public or private examples at step t, respectively. Then we have the spectral norm of reconstruction error*

$$\|\mathbf{R}\|_2 \leq \sqrt{2} s_{1,t} \mathbf{GSD}(V^{priv}, V^{pub}) + s_{k+1,t} \tag{1}$$

where $\mathbf{R} = \mathbf{G}_{priv} - \mathbf{G}_{priv} V^{pub} V^{pub\top}$ is the reconstruction error of private gradient matrix $\mathbf{G}_{priv}$ using public examples, $s_{1,t} \geq ... \geq s_{k,t} \geq ...$ are the singular values of $\mathbf{G}_{priv}$, $\mathbf{GSD}(V^{priv}, V^{pub})$ is the gradient subspace distance given by our algorithm.

Lemma 4.1 indicates that the reconstruction error of the private gradient matrix using public examples at step t is bounded by GSD, the subspace distance between the public and private gradient subspaces. A larger GSD may yield a larger reconstruction error at each step. Proof of this lemma can be found in Appendix E.

Theorem 4.2 (**Excess Risk**). *Assume that the loss $L(\mathbf{w}) = \frac{1}{n}\sum_{i=1}^{n} \ell(\mathbf{w}, z_i)$ is 1-Lipschitz, convex, and β-smooth. Let $\mathbf{w}^* = \operatorname{argmin}_{w \in \mathcal{W}} L(\mathbf{w})$. The excess risk of GEP obeys*

$$\mathbb{E}[L(\overline{\mathbf{w}})] - L(\mathbf{w}^*) \leq O\left(\frac{\sqrt{k\log(1/\delta)}}{n\epsilon}\right) + O\left(\frac{\sqrt{p\log(1/\delta)}}{n\epsilon}\overline{\mathbf{d}}\right) \tag{2}$$

*where GEP is (ϵ, δ)-DP (see Appendix A). Here we set $k = 1, \eta = \frac{1}{\beta}, T = \frac{n\beta\epsilon}{\sqrt{p}}$, $\overline{\mathbf{w}} = \frac{1}{T}\sum_{t=1}^{T} \mathbf{w}_t$, $\overline{\mathbf{d}} = \frac{1}{T}\sum_{t=1}^{T} d_t^2$, $d_t = \sqrt{2} s_{1,t} \mathbf{GSD} + s_{k+1,t}$, **GSD** is the gradient subspace distance when setting subspace dimension to 1, and s_t are singular values of the gradient matrix at step t.*

[1] In Appendix D.2, we empirically reconfirm that using the top subspace of the gradients themselves contains most of their signal.

Theorem 4.2 shows that the excess risk is affected by the GSD at each step. A larger GSD will result in a larger excess risk, which is often evaluated by the error rate in the experiments. In Appendix E, we show that without loss of generality, Theorem 4.2 can be extended to arbitrary subspace dimension k. Proof of this theorem can be found in Appendix E.

4.2 Ordering of GSD is Preserved over Training

Theorem 4.2 shows that the excess risk, measured by the error on the test set, can be predicted by GSD, assuming that we have *fresh* private examples at each step. However, this will cause significant privacy leakage and computational overhead if we repeatedly compute this distance using the whole private dataset.

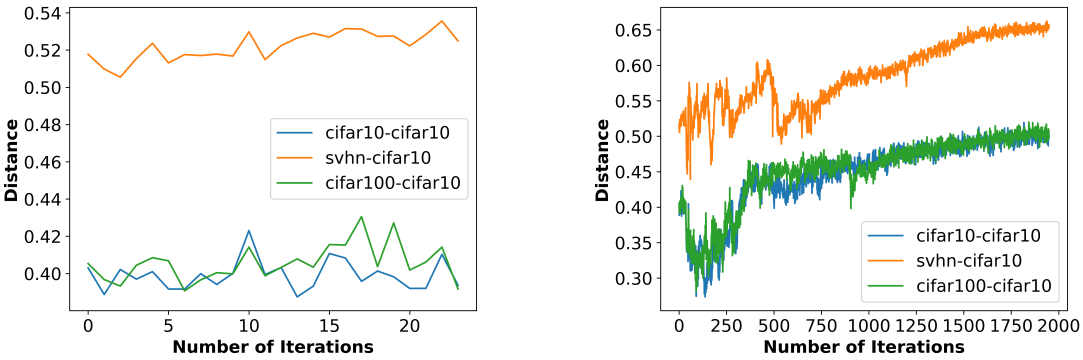

(a) Distance in 1 Epoch (b) Distance over 100 Epoch

Figure 1: The trend of distance during the process of training a ResNet20 model on CIFAR-10 using vanilla SGD. We follow a standard SGD training procedure and compute the distance between the current private batch and public examples at each iteration.

We empirically measure the GSD for each of the public datasets throughout the training process, as shown in Figure 1. This demonstrates that the relative ordering of the distances is preserved at almost all times. As a result, it suffices to compute each of the GSDs only once at initialization, requiring only one batch of examples from the private dataset and one pass through the model, incurring minimal data exposure and computational overhead. We can then select the dataset with the smallest GSD for use as our public dataset.

5 Second-Phase Pre-training

The standard method of private transfer learning consists of two phases: pre-training on a public dataset and fine-tuning on a private task. However, with large training sets and models, the computational burden of pre-training is prohibitive for most practitioners. Consequently, it is common to instead use pre-trained weights (obtained through pre-training on a fixed dataset) rather than run pre-training on a public dataset of choice. While this is computationally convenient, it limits the choice of pre-training datasets, and thus limits the accuracy in downstream fine-tuning.

$$\underbrace{f(\mathbf{W}_0; x) \xrightarrow{\mathbf{X}^{pub,1}} f(\mathbf{W}_{PT}; x)}_{\texttt{Load pre-trained weights}} \underbrace{\xrightarrow[\theta]{X_{pub,2}} f(\mathbf{W}_{PT}, \theta_0; x)}_{\texttt{Second-phase pre-training}} \underbrace{\xrightarrow{X_{priv}} f(\mathbf{W}_{PT}, \hat{\theta}; x)}_{\texttt{Private fine-tuning}}$$

Figure 2: Second-phase pre-training pipeline. We first choose a large model and download its pre-trained weights. Then we use an appropriate parameter-efficient fine-tuning mechanism and get trainable parameters θ. We train θ on a public dataset and get θ_0, called ***second-phase pre-training***. Finally, we pass θ_0 as the initial weights for private fine-tuning on the target task.

To alleviate this issue, we consider *second-phase pre-training*, in which a set of pre-trained weights are pre-trained on a second public dataset. We can then (privately) fine-tune the model on a sensitive dataset for the downstream task of interest. While this paradigm has previously been considered in the non-private setting Gururangan et al. (2020), to the best of our knowledge, we are the first to explore second phase pre-training in the differentially private setting. Pre-trained models may be significantly out of distribution with respect to the downstream task. Due to the noise introduced, the ability to adapt during fine-tuning may be diminished under differential privacy. Thus, the additional public data may be valuable for reducing the distribution shift. Second-phase pre-training is illustrated in Figure 2.

5.1 Second-Phase Pre-training Step by Step

Now we formally define second-phase pre-training. Suppose $f(\mathbf{W}_{pt}; x)$ where $\mathbf{W}_{pt}$ denotes pre-trained weights and x is input. To do second-phase pre-training, we first use a parameter-efficient fine-tuning mechanism and create new trainable parameters. Then we train these parameters on some public datasets. This step can be described by:

$$f_{2pt}\left(\mathbf{W}_{pt}, \theta; x_{pub}\right) \rightarrow \theta_0 \tag{3}$$

where x_{pub} are the public datasets and θ are the new trainable parameters, which are of far lower dimensionality than $\mathbf{W}$. We get the parameter vector θ_0 after this second-phase pre-training step. Finally, we initialize $\theta = \theta_0$ and privately fine-tune it by running DPSGD on the private task:

$$f_{ft}\left(\mathbf{W}_{pt}, \theta_0; x_{priv}\right) \rightarrow \hat{\theta} \tag{4}$$

Our experiments show that second-phase pre-training can give additional accuracy improvements, even when we only have a small number of public data examples. Furthermore, our distance measurement GSD remains a good indicator for choosing good public data for the second phase pre-training.

5.2 Parameter Efficiency in Private Fine-tuning

In both private and non-private settings, approaches frequently depart from the default of fine-tuning all model weights. For example, one can freeze parameters and fine-tune only specific layers, or introduce new parameters entirely. The resulting number of tunable parameters is almost always chosen to be smaller than during pre-training, leading to *parameter efficient* methods. This can be beneficial in terms of portability and resource requirements, and the fine-tuned model utility frequently matches or compares favorably to full fine-tuning. Parameter efficiency may be further advantageous in the differentially private setting, as it reduces the magnitude of noise one must introduce (though findings on the downstream impact on utility remain inconclusive). In the settings we consider, we will empirically find that parameter-efficient methods result in better utility.

In general, there are two ways of parameter-efficient fine-tuning. One approach is to select a subset of layers or parameters for fine-tuning. For instance, Bu et al. (2022) proposed fine-tuning only the bias terms of a model, which is both computationally and parameter-efficient while retaining similar accuracy compared to other methods. Another study by Cattan et al. (2022) found that fine-tuning the first and last layers of a model consistently improves its accuracy. The other approach is to freeze all existing parameters and add new trainable parameters during fine-tuning. Some examples include Adapter (Houlsby et al., 2019), Compacter (Mahabadi et al., 2021) and LoRA (Hu et al., 2022). Yu et al. (2022); Li et al. (2022c) demonstrated that private fine-tuning using parameter-efficient methods on large language models can be both computationally efficient and accurate.

6 Experiments

We explore the predictive power of GSD in both pre-conditioning and transfer learning settings. Specifically, we use GSD to choose a public dataset for GEP (Yu et al., 2021) and DP Mirror Descent (Amid et al., 2022)(representative of pre-conditioning methods) and second-phase pre-training (representative of transfer learning settings). We use a variety of datasets, including Fashion MNIST (Xiao et al., 2017), SVHN (Netzer

et al., 2011), and CIFAR-10 (Krizhevsky et al., 2009), as three canonical vision tasks. Based on the recommendations of Tramèr et al. (2022), we also evaluate our methods on datasets closer to privacy-sensitive applications. In particular, we also work with two medical image dataset: ChestX-ray14 (Wang et al., 2017) and HAM10000 (Tschandl, 2018). A variety of datasets are chosen as public data respectively. We evaluate our algorithms using both CNN-based (e.g., ResNet152 (He et al., 2016), DenseNet121 (Huang et al., 2017)) and Transformer-based (ViTs (Dosovitskiy et al., 2020)) architectures. A variety of parameter-efficient fine-tuning mechanisms are considered, including freezing layers and LoRA (Hu et al., 2022). Further details on our experimental setup appear in Appendix B.

We compute GSD non-privately using Algorithm 1, for two reasons. First, as discussed in Section 4, the privacy leakage due to hyperparameter selection is considered to be minimal and often disregarded in private ML. We thus treat selection via GSD similarly. Indeed, we experimentally validate that GSD has minimal impact on privacy using membership inference attacks in Section D.1. Second, beyond being a tool for public dataset selection, it is interesting in its own right to understand which metrics determine dataset utility in transfer settings.

Ideally, we would like our distance measure GSD to be model agnostic: it should depend only the two datasets, not on any particular model. This is not the case, since, as stated, our algorithms take gradients of the two datasets on the model of interest. However, we show that GSD is highly robust to changes in model architecture. We evaluate GSD on a 2-layer CNN (which we call a "probe network"), and show that relative ordering of GSDs is preserved, even though the architecture is far simpler than the models of interest.

We also compare our algorithm with Task2Vec (Achille et al., 2019), which has a similar goal as GSD. At a high level, Task2Vec represents a task (i.e., dataset) by transforming it into a vector so that the similarity between different datasets can be prescribed by the distance between two vectors. Although experiments show that Task2Vec matches taxonomic relations for datasets like iNaturalist (Horn et al., 2018), our empirical evaluation shows that it is outperformed by GSD in the differentially private setting. We also compare GSD with Optimal Transport Dataset Distance (OTDD) Alvarez-Melis & Fusi (2020), another algorithm that measures dataset similarity. Details are presented in Appendix.

6.1 Results for Pre-conditioning

We compute GSD and evaluate using GEP for the chosen datasets. The evaluation results are in Table 2. We find that, across a very wide range of different (and non-cherry-picked) private and public datasets, final accuracy is monotone as GSD decreases. Unexpectedly, we find that GSD between CIFAR-10 and CIFAR-100 is less than between CIFAR-10 and CIFAR-10. Nonetheless, this is predictive of final performance, where we see using CIFAR-100 as a public dataset is better than CIFAR-10, despite the fact that the private dataset is also CIFAR-10. In particular, this supports our use of a rigorous metric to predict dataset suitability rather than going off intuition (which this example shows can be incorrect).

For ChestX-ray14, we use AUC instead of prediction accuracy because of high class imbalance. The evaluation results are given in Table 1. Once again, lower GSD implies higher model utility. We see that ChestX-ray14 is the best public dataset, but the second best is another chest x-ray dataset. Furthermore, using a significantly different dataset (CIFAR-100) as the public dataset results in worse utility than using no public dataset at all.

We include further experiments in the appendix: 1) evaluation on DP Mirror Descent, in Appendix D.3; and 2) combining multiple public datasets, in Appendix D.8.

6.2 Results for Second-Phase Pre-training

We compute the GSD and evaluate using second-phase pre-training for the chosen datasets. The evaluation results are given in Table 3. As before, we consistently find that smaller GSD leads to larger utility. Like ChestX-ray14, HAM10000 is highly imbalanced, so we again use AUC. However, unlike ChestX-ray14, which contains roughly 100,000 images, HAM10000 is relatively small (only 10,000 skin lesion images). We assume that we can only collect 300 images from it and treat them as public. As shown in Table 3, even this small public dataset can boost the utility through second-phase pre-training. While even the worst public dataset does not dramatically hurt utility (in contrast to the pre-conditioning setting), GSD can still be a good

Table 2: GEP evaluation accuracy and corresponding distance in descending order. We use the *same* model for private training and GSD computation. "-" means DP-SGD without public data. We use $\epsilon = 2, \delta = 1e-5$.

Accuracy	Private Dataset	Public Dataset	Distance
58.63%	CIFAR-10	CIFAR-100	**0.20**
57.64%		CIFAR-10	0.24
56.75%		SVHN	0.28
52.16%		-	-
91.32%	SVHN	SVHN	**0.25**
89.29%		CIFAR-100	0.31
89.08%		MNIST-M	0.39
83.21%		-	-
85.25%	FMNIST	FMNIST	**0.34**
84.54%		FLOWER	0.43
83.91%		MNIST	0.50
79.77%		-	-

indicator of the utility of public datasets. Similar results apply when we evaluate second-phase pre-training and GSD on ChestX-ray14 using ViTs, as shown in Appendix D.4.

Table 3: Second-Phase evaluation results and corresponding distance in descending order. We use DenseNet121 and choose two convolutional layers and the last layer for second-phase pre-training and private fine-tuning. Detailed settings can be found in Appendix B. We use the *same* model setting for private training and distance computation. "-" means DP-SGD training. We use $\epsilon = 2, \delta = 1e-5$.

AUC	Private Dataset	Public Dataset	Distance
87.06%	HAM10000	HAM10000	**0.50**
85.53%		KagSkin	0.68
85.40%		-	-
84.92%		CIFAR-100	0.73
84.88%		KagChest	0.73

6.3 Transferability: Simple Models Remain Predictive

Our empirical evaluation suggests that GSD is transferable over different architectures. In previous experiments, we used the same model architecture for both GSD and the (private) learning algorithm. We find that the relative GSD ordering of different public datasets is robust across different architectures. For example, ***GSD***(ChestX-ray14, KagChest) is consistently smaller than ***GSD***(ChestX-ray14, CIFAR-100), no matter what model architecture or parameter-efficient fine-tuning mechanism we choose. Inspired by this finding, we measure GSD with a very simple CNN, which we call a "probe network." It consists of two convolutional layers and one linear layer, with roughly 30,000 parameters. Evaluation results are given in Appendix D.5. They demonstrate that even using a simple CNN, GSD can still derive accurate distance measurement with regard to the utility of public data for private learning tasks. The similarity described by GSD is thus robust against the choice of model architecture.

6.4 Task2Vec May Give Wrong Predictions

Result. We evaluate the similarity between each public-private dataset pair using Task2Vec Achille et al. (2019). Task2Vec gives similarity results of mixed quality: to highlight one notable failure case, we consider the ChestX-ray14 private dataset in Table 4. The closest dataset is itself. However, following this, CIFAR-100 is as close as KagChest, while it is qualitatively very different from ChestX-ray14 and provides low utility

Table 4: Results for GSD vs. Task2Vec. We evaluate ChestX-ray14 using GEP and compute the distance using Task2Vec and GSD. As suggested by Task2Vec, CIFAR-100 should be as close to ChestX-ray14 as KagChest, while it actually provides low utility.

	AUC	Task2Vec	GSD
ChestX-ray14	69.02%	0.052	0.15
KagChest	66.62%	0.16	0.36
-	64.90%	-	-
CIFAR-100	48.80%	0.16	0.55

when used as the public dataset. In contrast, GSD orders the quality of these datasets in a manner consistent with their quality. We find similar discrepancies for HAM10000, results are given in the Appendix D.7.

7 Limitations and Discussions

We note that, as stated, GSD is not differentially private, as it interacts with the unprotected gradients of the private data. For our scientific question, exploring which public datasets perform well for a particular private task, this is inconsequential. For the algorithmic problem of actually selecting a public dataset for use, one may fear that choosing a public dataset based on GSD may leak sensitive information about the private dataset. However, we remind that the selection of a public dataset is a hyperparameter: in essentially all work on private ML, hyperparameter tuning is performed non-privately, since the privacy impact is considered to be minimal (Papernot & Steinke, 2022; Mohapatra et al., 2022). Thus, for the purpose of our scientific exploration and to be comparable with the majority of the private ML literature, our experiments are performed with non-private computation of GSD. However, we nonetheless discuss differentially private methods for GSD computation in Appendix C. Furthermore, in Appendix D.1, we empirically evaluate the privacy leakage of GSD under a number of membership inference attacks, and even with very strong assumptions on the attacker, they are unable to mount effective attacks. We leave the development of a practical method with rigorous DP guarantees for future work.

8 Conclusion

A recent line of work explores the power of public data in private machine learning. However, we do not yet have a good understanding of which public datasets are more or less effective for a particular private task, and thus how to select them. We propose a new distance GSD, and empirically demonstrate that lower GSD of a public dataset is strongly predictive of higher downstream utility. Our algorithms require minimal data and are computationally efficient. Additionally, transferability of GSD demonstrates that it is generally model agnostic, allowing one to decouple the public dataset selection and private learning. We further demonstrate that GSD is effective for predicting utility in settings involving both pre-conditioning and second-phase pre-training, and that GSD compares favorably to other measures of dataset distance.

References

Martin Abadi, Andy Chu, Ian Goodfellow, H. Brendan McMahan, Ilya Mironov, Kunal Talwar, and Li Zhang. Deep learning with differential privacy. In *Proceedings of the 2016 ACM SIGSAC Conference on Computer and Communications Security*, CCS '16, pp. 308–318, New York, NY, USA, 2016. Association for Computing Machinery. ISBN 9781450341394. doi: 10.1145/2976749.2978318. URL `https://doi.org/10.1145/2976749.2978318`.

Alessandro Achille, Michael Lam, Rahul Tewari, Avinash Ravichandran, Subhransu Maji, Charless C. Fowlkes, Stefano Soatto, and Pietro Perona. Task2vec: Task embedding for meta-learning. In *2019 IEEE/CVF International Conference on Computer Vision, ICCV 2019, Seoul, Korea (South), October 27 - November 2, 2019*, pp. 6429–6438. IEEE, 2019. doi: 10.1109/ICCV.2019.00653. URL `https://doi.org/10.1109/ICCV.2019.00653`.

Sozan Mohammed Ahmed and Ramadhan J. Mstafa. Identifying severity grading of knee osteoarthritis from x-ray images using an efficient mixture of deep learning and machine learning models. *Diagnostics*, 12(12), 2022. ISSN 2075-4418. doi: 10.3390/diagnostics12122939. URL https://www.mdpi.com/2075-4418/12/12/2939.

David Alvarez-Melis and Nicoló Fusi. Geometric dataset distances via optimal transport. *CoRR*, abs/2002.02923, 2020. URL https://arxiv.org/abs/2002.02923.

Ehsan Amid, Arun Ganesh, Rajiv Mathews, Swaroop Ramaswamy, Shuang Song, Thomas Steinke, Thomas Steinke, Vinith M Suriyakumar, Om Thakkar, and Abhradeep Thakurta. Public data-assisted mirror descent for private model training. In Kamalika Chaudhuri, Stefanie Jegelka, Le Song, Csaba Szepesvari, Gang Niu, and Sivan Sabato (eds.), *Proceedings of the 39th International Conference on Machine Learning*, volume 162 of *Proceedings of Machine Learning Research*, pp. 517–535. PMLR, 17–23 Jul 2022. URL https://proceedings.mlr.press/v162/amid22a.html.

Raef Bassily, Adam D. Smith, and Abhradeep Thakurta. Private empirical risk minimization: Efficient algorithms and tight error bounds. In *55th IEEE Annual Symposium on Foundations of Computer Science, FOCS 2014, Philadelphia, PA, USA, October 18-21, 2014*, pp. 464–473. IEEE Computer Society, 2014. doi: 10.1109/FOCS.2014.56. URL https://doi.org/10.1109/FOCS.2014.56.

Shai Ben-David, John Blitzer, Koby Crammer, and Fernando Pereira. Analysis of representations for domain adaptation. In Bernhard Schölkopf, John C. Platt, and Thomas Hofmann (eds.), *Advances in Neural Information Processing Systems 19, Proceedings of the Twentieth Annual Conference on Neural Information Processing Systems, Vancouver, British Columbia, Canada, December 4-7, 2006*, pp. 137–144. MIT Press, 2006. URL https://proceedings.neurips.cc/paper/2006/hash/b1b0432ceafb0ce714426e9114852ac7-Abstract.html.

Shai Ben-David, John Blitzer, Koby Crammer, Alex Kulesza, Fernando Pereira, and Jennifer Wortman Vaughan. A theory of learning from different domains. *Mach. Learn.*, 79(1-2):151–175, 2010. doi: 10.1007/s10994-009-5152-4. URL https://doi.org/10.1007/s10994-009-5152-4.

Tom Brown, Benjamin Mann, Nick Ryder, Melanie Subbiah, Jared D Kaplan, Prafulla Dhariwal, Arvind Neelakantan, Pranav Shyam, Girish Sastry, Amanda Askell, Sandhini Agarwal, Ariel Herbert-Voss, Gretchen Krueger, Tom Henighan, Rewon Child, Aditya Ramesh, Daniel Ziegler, Jeffrey Wu, Clemens Winter, Chris Hesse, Mark Chen, Eric Sigler, Mateusz Litwin, Scott Gray, Benjamin Chess, Jack Clark, Christopher Berner, Sam McCandlish, Alec Radford, Ilya Sutskever, and Dario Amodei. Language models are few-shot learners. In H. Larochelle, M. Ranzato, R. Hadsell, M.F. Balcan, and H. Lin (eds.), *Advances in Neural Information Processing Systems*, volume 33, pp. 1877–1901. Curran Associates, Inc., 2020. URL https://proceedings.neurips.cc/paper_files/paper/2020/file/1457c0d6bfcb4967418bfb8ac142f64a-Paper.pdf.

Zhiqi Bu, Yu-Xiang Wang, Sheng Zha, and George Karypis. Differentially private bias-term only fine-tuning of foundation models, 2022. URL https://arxiv.org/abs/2210.00036.

Nicholas Carlini, Florian Tramèr, Eric Wallace, Matthew Jagielski, Ariel Herbert-Voss, Katherine Lee, Adam Roberts, Tom Brown, Dawn Song, Úlfar Erlingsson, Alina Oprea, and Colin Raffel. Extracting training data from large language models. In *30th USENIX Security Symposium (USENIX Security 21)*, pp. 2633–2650. USENIX Association, August 2021. ISBN 978-1-939133-24-3. URL https://www.usenix.org/conference/usenixsecurity21/presentation/carlini-extracting.

Yannis Cattan, Christopher A. Choquette-Choo, Nicolas Papernot, and Abhradeep Thakurta. Fine-tuning with differential privacy necessitates an additional hyperparameter search, 2022. URL https://arxiv.org/abs/2210.02156.

Kamalika Chaudhuri, Anand D. Sarwate, and Kaushik Sinha. A near-optimal algorithm for differentially-private principal components. *J. Mach. Learn. Res.*, 14(1):2905–2943, 2013. doi: 10.5555/2567709.2567754. URL https://dl.acm.org/doi/10.5555/2567709.2567754.

Yasuko Chikuse. *Statistics on special manifolds*, volume 174. Springer Science & Business Media, 2003.

J. H. Conway, R. H. Hardin, and N. J. A. Sloane. Packing lines, planes, etc.: Packings in grassmannian space. 2002. doi: 10.48550/ARXIV.MATH/0208004. URL https://arxiv.org/abs/math/0208004.

Soham De, Leonard Berrada, Jamie Hayes, Samuel L Smith, and Borja Balle. Unlocking high-accuracy differentially private image classification through scale. *arXiv preprint arXiv:2204.13650*, 2022.

Paulo Eduardo de Aguiar Kuriki, Eduardo Farina, Nitamar Abdala, Bruno Aragão, Marcelo Coelho, Marcelo Takahashi Straus, Gabriel Bianco, and Felipe Campos Kitamura, 2023. URL https://www.kaggle.com/dsv/5142976.

J. Deng, W. Dong, R. Socher, L.-J. Li, K. Li, and L. Fei-Fei. ImageNet: A Large-Scale Hierarchical Image Database. In *CVPR09*, 2009.

Alexey Dosovitskiy, Lucas Beyer, Alexander Kolesnikov, Dirk Weissenborn, Xiaohua Zhai, Thomas Unterthiner, Mostafa Dehghani, Matthias Minderer, Georg Heigold, Sylvain Gelly, Jakob Uszkoreit, and Neil Houlsby. An image is worth 16x16 words: Transformers for image recognition at scale. *CoRR*, abs/2010.11929, 2020. URL https://arxiv.org/abs/2010.11929.

Cynthia Dwork, Frank McSherry, Kobbi Nissim, and Adam Smith. Calibrating noise to sensitivity in private data analysis. In Shai Halevi and Tal Rabin (eds.), *Theory of Cryptography*, pp. 265–284, Berlin, Heidelberg, 2006. Springer Berlin Heidelberg. ISBN 978-3-540-32732-5.

Cynthia Dwork, Kunal Talwar, Abhradeep Thakurta, and Li Zhang. Analyze gauss: optimal bounds for privacy-preserving principal component analysis. In David B. Shmoys (ed.), *Symposium on Theory of Computing, STOC 2014, New York, NY, USA, May 31 - June 03, 2014*, pp. 11–20. ACM, 2014. doi: 10.1145/2591796.2591883. URL https://doi.org/10.1145/2591796.2591883.

Carl Eckart and Gale Young. The approximation of one matrix by another of lower rank. *Psychometrika*, 1 (3):211–218, 1936.

Alan Edelman, Tomás A. Arias, and Steven Thomas Smith. The geometry of algorithms with orthogonality constraints. *SIAM J. Matrix Anal. Appl.*, 20(2):303–353, 1998. doi: 10.1137/S0895479895290954. URL https://doi.org/10.1137/S0895479895290954.

Claudio Fanconi. Skin cancer: Malignant vs. benign, June 2019.

Matt Fredrikson, Somesh Jha, and Thomas Ristenpart. Model inversion attacks that exploit confidence information and basic countermeasures. In *Proceedings of the 22nd ACM SIGSAC Conference on Computer and Communications Security*, CCS '15, pp. 1322–1333, New York, NY, USA, 2015. Association for Computing Machinery. ISBN 9781450338325. doi: 10.1145/2810103.2813677. URL https://doi.org/10.1145/2810103.2813677.

Virginie Gabrel, Cécile Murat, and Aurélie Thiele. Recent advances in robust optimization: An overview. *European journal of operational research*, 235(3):471–483, 2014.

Arun Ganesh, Mahdi Haghifam, Milad Nasr, Sewoong Oh, Thomas Steinke, Om Thakkar, Abhradeep Guha Thakurta, and Lun Wang. Why is public pretraining necessary for private model training? In Andreas Krause, Emma Brunskill, Kyunghyun Cho, Barbara Engelhardt, Sivan Sabato, and Jonathan Scarlett (eds.), *Proceedings of the 40th International Conference on Machine Learning*, volume 202 of *Proceedings of Machine Learning Research*, pp. 10611–10627. PMLR, 23–29 Jul 2023. URL https://proceedings.mlr.press/v202/ganesh23a.html.

Yaroslav Ganin, Evgeniya Ustinova, Hana Ajakan, Pascal Germain, Hugo Larochelle, François Laviolette, Mario Marchand, and Victor S. Lempitsky. Domain-adversarial training of neural networks. *J. Mach. Learn. Res.*, 17:59:1–59:35, 2016. URL http://jmlr.org/papers/v17/15-239.html.

Aditya Golatkar, Alessandro Achille, Yu-Xiang Wang, Aaron Roth, Michael Kearns, and Stefano Soatto. Mixed differential privacy in computer vision. *CoRR*, abs/2203.11481, 2022. doi: 10.48550/arXiv.2203.11481. URL https://doi.org/10.48550/arXiv.2203.11481.

Gene H. Golub and Charles F. Van Loan. *Matrix Computations, Third Edition*. Johns Hopkins University Press, 1996. ISBN 978-0-8018-5414-9.

Guy Gur-Ari, Daniel A. Roberts, and Ethan Dyer. Gradient descent happens in a tiny subspace. *CoRR*, abs/1812.04754, 2018. URL http://arxiv.org/abs/1812.04754.

Suchin Gururangan, Ana Marasovic, Swabha Swayamdipta, Kyle Lo, Iz Beltagy, Doug Downey, and Noah A. Smith. Don't stop pretraining: Adapt language models to domains and tasks. In Dan Jurafsky, Joyce Chai, Natalie Schluter, and Joel R. Tetreault (eds.), *Proceedings of the 58th Annual Meeting of the Association for Computational Linguistics, ACL 2020, Online, July 5-10, 2020*, pp. 8342–8360. Association for Computational Linguistics, 2020. doi: 10.18653/v1/2020.acl-main.740. URL https://doi.org/10.18653/v1/2020.acl-main.740.

Jihun Ham and Daniel D. Lee. Grassmann discriminant analysis: a unifying view on subspace-based learning. In William W. Cohen, Andrew McCallum, and Sam T. Roweis (eds.), *Machine Learning, Proceedings of the Twenty-Fifth International Conference (ICML 2008), Helsinki, Finland, June 5-9, 2008*, volume 307 of *ACM International Conference Proceeding Series*, pp. 376–383. ACM, 2008. doi: 10.1145/1390156.1390204. URL https://doi.org/10.1145/1390156.1390204.

Kaiming He, Xiangyu Zhang, Shaoqing Ren, and Jian Sun. Deep residual learning for image recognition. In *2016 IEEE Conference on Computer Vision and Pattern Recognition, CVPR 2016, Las Vegas, NV, USA, June 27-30, 2016*, pp. 770–778. IEEE Computer Society, 2016. doi: 10.1109/CVPR.2016.90. URL https://doi.org/10.1109/CVPR.2016.90.

Grant Van Horn, Oisin Mac Aodha, Yang Song, Yin Cui, Chen Sun, Alexander Shepard, Hartwig Adam, Pietro Perona, and Serge J. Belongie. The inaturalist species classification and detection dataset. In *2018 IEEE Conference on Computer Vision and Pattern Recognition, CVPR 2018, Salt Lake City, UT, USA, June 18-22, 2018*, pp. 8769–8778. Computer Vision Foundation / IEEE Computer Society, 2018. doi: 10.1109/CVPR.2018.00914. URL http://openaccess.thecvf.com/content_cvpr_2018/html/Van_Horn_The_INaturalist_Species_CVPR_2018_paper.html.

Neil Houlsby, Andrei Giurgiu, Stanislaw Jastrzebski, Bruna Morrone, Quentin De Laroussilhe, Andrea Gesmundo, Mona Attariyan, and Sylvain Gelly. Parameter-efficient transfer learning for NLP. In Kamalika Chaudhuri and Ruslan Salakhutdinov (eds.), *Proceedings of the 36th International Conference on Machine Learning*, volume 97 of *Proceedings of Machine Learning Research*, pp. 2790–2799. PMLR, 09–15 Jun 2019. URL https://proceedings.mlr.press/v97/houlsby19a.html.

Edward J Hu, yelong shen, Phillip Wallis, Zeyuan Allen-Zhu, Yuanzhi Li, Shean Wang, Lu Wang, and Weizhu Chen. LoRA: Low-rank adaptation of large language models. In *International Conference on Learning Representations*, 2022. URL https://openreview.net/forum?id=nZeVKeeFYf9.

Gao Huang, Zhuang Liu, Laurens van der Maaten, and Kilian Q. Weinberger. Densely connected convolutional networks. In *2017 IEEE Conference on Computer Vision and Pattern Recognition, CVPR 2017, Honolulu, HI, USA, July 21-26, 2017*, pp. 2261–2269. IEEE Computer Society, 2017. doi: 10.1109/CVPR.2017.243. URL https://doi.org/10.1109/CVPR.2017.243.

Jeremy Irvin, Pranav Rajpurkar, Michael Ko, Yifan Yu, Silviana Ciurea-Ilcus, Chris Chute, Henrik Marklund, Behzad Haghgoo, Robyn Ball, Katie Shpanskaya, Jayne Seekins, David A. Mong, Safwan S. Halabi, Jesse K. Sandberg, Ricky Jones, David B. Larson, Curtis P. Langlotz, Bhavik N. Patel, Matthew P. Lungren, and Andrew Y. Ng. Chexpert: A large chest radiograph dataset with uncertainty labels and expert comparison, 2019. URL https://arxiv.org/abs/1901.07031.

Peter Kairouz, Mónica Ribero, Keith Rush, and Abhradeep Thakurta. Dimension independence in unconstrained private ERM via adaptive preconditioning. *CoRR*, abs/2008.06570, 2020. URL https://arxiv.org/abs/2008.06570.

Peter Kairouz, Mónica Ribero, Keith Rush, and Abhradeep Thakurta. (nearly) dimension independent private ERM with adagrad rates via publicly estimated subspaces. In *Proceedings of the 34th Annual Conference on Learning Theory*, COLT '21, pp. 2717–2746, 2021.

Daniel S. Kermany, Michael Goldbaum, Wenjia Cai, Carolina C.S. Valentim, Huiying Liang, Sally L. Baxter, Alex McKeown, Ge Yang, Xiaokang Wu, Fangbing Yan, Justin Dong, Made K. Prasadha, Jacqueline Pei, Magdalene Y.L. Ting, Jie Zhu, Christina Li, Sierra Hewett, Jason Dong, Ian Ziyar, Alexander Shi, Runze Zhang, Lianghong Zheng, Rui Hou, William Shi, Xin Fu, Yaou Duan, Viet A.N. Huu, Cindy Wen, Edward D. Zhang, Charlotte L. Zhang, Oulan Li, Xiaobo Wang, Michael A. Singer, Xiaodong Sun, Jie Xu, Ali Tafreshi, M. Anthony Lewis, Huimin Xia, and Kang Zhang. Identifying medical diagnoses and treatable diseases by image-based deep learning. *Cell*, 172(5):1122–1131.e9, 2018. ISSN 0092-8674. doi: https://doi.org/10.1016/j.cell.2018.02.010. URL https://www.sciencedirect.com/science/article/pii/S0092867418301545.

Alex Krizhevsky, Geoffrey Hinton, et al. Learning multiple layers of features from tiny images. 2009.

Jaewoo Lee and Daniel Kifer. Concentrated differentially private gradient descent with adaptive per-iteration privacy budget. In Yike Guo and Faisal Farooq (eds.), *Proceedings of the 24th ACM SIGKDD International Conference on Knowledge Discovery & Data Mining, KDD 2018, London, UK, August 19-23, 2018*, pp. 1656–1665. ACM, 2018. doi: 10.1145/3219819.3220076. URL https://doi.org/10.1145/3219819.3220076.

Tian Li, Manzil Zaheer, Sashank Reddi, and Virginia Smith. Private adaptive optimization with side information. In Kamalika Chaudhuri, Stefanie Jegelka, Le Song, Csaba Szepesvari, Gang Niu, and Sivan Sabato (eds.), *Proceedings of the 39th International Conference on Machine Learning*, volume 162 of *Proceedings of Machine Learning Research*, pp. 13086–13105. PMLR, 17–23 Jul 2022a. URL https://proceedings.mlr.press/v162/li22x.html.

Xinyan Li, Qilong Gu, Yingxue Zhou, Tiancong Chen, and Arindam Banerjee. Hessian based analysis of SGD for deep nets: Dynamics and generalization. In Carlotta Demeniconi and Nitesh V. Chawla (eds.), *Proceedings of the 2020 SIAM International Conference on Data Mining, SDM 2020, Cincinnati, Ohio, USA, May 7-9, 2020*, pp. 190–198. SIAM, 2020. doi: 10.1137/1.9781611976236.22. URL https://doi.org/10.1137/1.9781611976236.22.

Xuechen Li, Daogao Liu, Tatsunori Hashimoto, Huseyin A. Inan, Janardhan Kulkarni, Yin Tat Lee, and Abhradeep Guha Thakurta. When does differentially private learning not suffer in high dimensions? *CoRR*, abs/2207.00160, 2022b. doi: 10.48550/arXiv.2207.00160. URL https://doi.org/10.48550/arXiv.2207.00160.

Xuechen Li, Florian Tramèr, Percy Liang, and Tatsunori Hashimoto. Large language models can be strong differentially private learners. In *Proceedings of the 10th International Conference on Learning Representations*, ICLR '22, 2022c.

Xiyang Liu, Weihao Kong, Prateek Jain, and Sewoong Oh. DP-PCA: Statistically optimal and differentially private PCA. In Alice H. Oh, Alekh Agarwal, Danielle Belgrave, and Kyunghyun Cho (eds.), *Advances in Neural Information Processing Systems*, 2022. URL https://openreview.net/forum?id=rZalM6vZ2J.

Zelun Luo, Daniel J. Wu, Ehsan Adeli, and Li Fei-Fei. Scalable differential privacy with sparse network finetuning. In *IEEE Conference on Computer Vision and Pattern Recognition, CVPR 2021, virtual, June 19-25, 2021*, pp. 5059–5068. Computer Vision Foundation / IEEE, 2021. doi: 10.1109/CVPR46437.2021.00502. URL https://openaccess.thecvf.com/content/CVPR2021/html/Luo_Scalable_Differential_Privacy_With_Sparse_Network_Finetuning_CVPR_2021_paper.html.

Rabeeh Karimi Mahabadi, James Henderson, and Sebastian Ruder. Compacter: Efficient low-rank hypercomplex adapter layers. In Marc'Aurelio Ranzato, Alina Beygelzimer, Yann N. Dauphin, Percy Liang, and Jennifer Wortman Vaughan (eds.), *Advances in Neural Information Processing Systems 34: Annual Conference on Neural Information Processing Systems 2021, NeurIPS 2021, December 6-14, 2021, virtual*, pp. 1022–1035, 2021. URL https://proceedings.neurips.cc/paper/2021/hash/081be9fdff07f3bc808f935906ef70c0-Abstract.html.

Harsh Mehta, Abhradeep Thakurta, Alexey Kurakin, and Ashok Cutkosky. Large scale transfer learning for differentially private image classification. *arXiv preprint arXiv:2205.02973*, 2022.

Shubhankar Mohapatra, Sajin Sasy, Xi He, Gautam Kamath, and Om Thakkar. The role of adaptive optimizers for honest private hyperparameter selection. In *Proceedings of the Thirty-Sixth AAAI Conference on Artificial Intelligence*, volume 36 of *AAAI '22*, pp. 7806–7813, 2022.

Milad Nasr, Reza Shokri, and Amir Houmansadr. Comprehensive privacy analysis of deep learning: Passive and active white-box inference attacks against centralized and federated learning. In *2019 IEEE Symposium on Security and Privacy (SP)*, pp. 739–753, 2019. doi: 10.1109/SP.2019.00065.

Milad Nasr, Saeed Mahloujifar, Xinyu Tang, Prateek Mittal, and Amir Houmansadr. Effectively using public data in privacy preserving machine learning. In Andreas Krause, Emma Brunskill, Kyunghyun Cho, Barbara Engelhardt, Sivan Sabato, and Jonathan Scarlett (eds.), *Proceedings of the 40th International Conference on Machine Learning*, volume 202 of *Proceedings of Machine Learning Research*, pp. 25718–25732. PMLR, 23–29 Jul 2023. URL `https://proceedings.mlr.press/v202/nasr23a.html`.

Yuval Netzer, Tao Wang, Adam Coates, Alessandro Bissacco, Bo Wu, and Andrew Y Ng. Reading digits in natural images with unsupervised feature learning. 2011.

Maria-Irina Nicolae, Mathieu Sinn, Minh Ngoc Tran, Beat Buesser, Ambrish Rawat, Martin Wistuba, Valentina Zantedeschi, Nathalie Baracaldo, Bryant Chen, Heiko Ludwig, Ian Molloy, and Ben Edwards. Adversarial robustness toolbox v1.2.0. *CoRR*, 1807.01069, 2018. URL `https://arxiv.org/pdf/1807.01069`.

Maria-Elena Nilsback and Andrew Zisserman. Automated flower classification over a large number of classes. In *Indian Conference on Computer Vision, Graphics and Image Processing*, Dec 2008.

Nicolas Papernot and Thomas Steinke. Hyperparameter tuning with renyi differential privacy. In *Proceedings of the 10th International Conference on Learning Representations*, ICLR '22, 2022.

Reza Shokri, Marco Stronati, Congzheng Song, and Vitaly Shmatikov. Membership inference attacks against machine learning models. In *2017 IEEE Symposium on Security and Privacy (SP)*, pp. 3–18, 2017. doi: 10.1109/SP.2017.41.

Shuang Song, Kamalika Chaudhuri, and Anand D. Sarwate. Stochastic gradient descent with differentially private updates. In *IEEE Global Conference on Signal and Information Processing, GlobalSIP 2013, Austin, TX, USA, December 3-5, 2013*, pp. 245–248. IEEE, 2013. doi: 10.1109/GlobalSIP.2013.6736861. URL `https://doi.org/10.1109/GlobalSIP.2013.6736861`.

Florian Tramèr, Gautam Kamath, and Nicholas Carlini. Considerations for differentially private learning with large-scale public pretraining. *arXiv preprint arXiv:2212.06470*, 2022.

Philipp Tschandl. The HAM10000 dataset, a large collection of multi-source dermatoscopic images of common pigmented skin lesions, 2018. URL `https://doi.org/10.7910/DVN/DBW86T`.

Dequan Wang, Evan Shelhamer, Shaoteng Liu, Bruno Olshausen, and Trevor Darrell. Tent: Fully test-time adaptation by entropy minimization. In *International Conference on Learning Representations*, 2021. URL `https://openreview.net/forum?id=uXl3bZLkr3c`.

Mei Wang and Weihong Deng. Deep visual domain adaptation: A survey. *Neurocomputing*, 312:135–153, 2018. doi: 10.1016/j.neucom.2018.05.083. URL `https://doi.org/10.1016/j.neucom.2018.05.083`.

Xiaosong Wang, Yifan Peng, Le Lu, Zhiyong Lu, Mohammadhadi Bagheri, and Ronald Summers. Chestx-ray8: Hospital-scale chest x-ray database and benchmarks on weakly-supervised classification and localization of common thorax diseases. In *2017 IEEE Conference on Computer Vision and Pattern Recognition(CVPR)*, pp. 3462–3471, 2017.

Han Xiao, Kashif Rasul, and Roland Vollgraf. Fashion-mnist: a novel image dataset for benchmarking machine learning algorithms. *CoRR*, abs/1708.07747, 2017. URL `http://arxiv.org/abs/1708.07747`.

Da Yu, Huishuai Zhang, Wei Chen, and Tie-Yan Liu. Do not let privacy overbill utility: Gradient embedding perturbation for private learning. In *9th International Conference on Learning Representations, ICLR 2021, Virtual Event, Austria, May 3-7, 2021*. OpenReview.net, 2021. URL `https://openreview.net/forum?id=7aogOj_VYOO`.

Da Yu, Saurabh Naik, Arturs Backurs, Sivakanth Gopi, Huseyin A Inan, Gautam Kamath, Janardhan Kulkarni, Yin Tat Lee, Andre Manoel, Lukas Wutschitz, Sergey Yekhanin, and Huishuai Zhang. Differentially private fine-tuning of language models. In *Proceedings of the 10th International Conference on Learning Representations*, ICLR '22, 2022.

Da Yu, Sivakanth Gopi, Janardhan Kulkarni, Zinan Lin, Saurabh Naik, Tomasz Lukasz Religa, Jian Yin, and Huishuai Zhang. Selective pre-training for private fine-tuning, 2023.

Lei Zhang. Transfer adaptation learning: A decade survey. *CoRR*, abs/1903.04687, 2019. URL `http://arxiv.org/abs/1903.04687`.

Yingxue Zhou, Steven Wu, and Arindam Banerjee. Bypassing the ambient dimension: Private {sgd} with gradient subspace identification. In *International Conference on Learning Representations*, 2021. URL `https://openreview.net/forum?id=7dpmlkBuJFC`.

Fuzhen Zhuang, Zhiyuan Qi, Keyu Duan, Dongbo Xi, Yongchun Zhu, Hengshu Zhu, Hui Xiong, and Qing He. A comprehensive survey on transfer learning. *CoRR*, abs/1911.02685, 2019. URL `http://arxiv.org/abs/1911.02685`.

A Missing Preliminaries

Definition 4 ((ρ, η)-close). *A randomized algorithm $\mathcal{A}(.)$ that outputs an approximate distance between to subspaces span(V_1) and span(V_2), $\hat{d}(V_1, V_2)$, is an* (ρ, η)-close *approximation to the true subspace distance $d(V_1, V_2)$, if they satisfy:*

$$\Pr\left[|\hat{d}(V_1, V_2) - d(V_1, V_2)| \leq \rho\right] \geq 1 - \eta.$$

Gradient Embedding Perturbation (GEP). Our theoretical analysis is based on GEP, the state-of-the-art private learning algorithm that leverages public data. Here we briefly introduce their algorithm. GEP involves three steps: 1) it computes a set of the orthonormal basis for the lower-dimensional subspace; 2) GEP projects the private gradients to the subspace derived from step 1, thus dividing the private gradients into two parts: embedding gradients that contain most of the information carried by the gradient, and the remainder are called residual gradients; 3) GEP clips two parts of the gradients separately and perturbs them to achieve differential privacy.

Algorithm 2 Gradient Embedding Perturbation (GEP)

Input: Private dataset X_{priv}, public examples x_{pub}, loss function $\mathcal{L}$, model weights $\boldsymbol{\theta}_0$, dimension k, learning rate η, number of iterations T, noise multiplier σ_1, σ_2, clip norm S_1, S_2 **Output:** Differentially private model $\boldsymbol{\theta}_T$

for $t = 1 \cdots T$ **do**
  Compute per-sample gradient matrix G_t^{priv} and public gradient matrix G_t^{pub}
  `// Compute an orthonormal basis for the public subspace`
  Initialize $V_k^{pub} \in \mathbb{R}^{k \times p}$ randomly.
  for $i = 1 \cdots T_{power}$ **do**
    Compute $A = G_t^{pub} V_k^{pub\top}$ and $V_k^{pub} = A^\top V_k^{pub\top}$
    Orthogonalize V_k^{pub} and normalize row vectors.
  end for
  Delete G_t^{pub} to free memory.
  `// Project the private gradients onto public subspace`
  Compute gradient embedding $W_t = G_t^{priv} V_{k,t}^{pub\top}$ and clip its rows with S_1 to obtain $\hat{W}$.
  Compute residual gradients $R_t = G_t^{priv} - W_t V_{k,t}^{pub}$ and clip its rows with S_2 to obtain $\hat{R}$.
  `// Perturb gradient embedding and residual gradient separately`
  Perturb embedding with noise $\boldsymbol{z}_t^{(1)} \sim \mathcal{N}\left(0, \sigma_1^2 \boldsymbol{I}_k\right)$: w_t :=sum over rows of $\hat{W}_t$, $\hat{w}_t := w_t + \boldsymbol{z}_t^{(1)}$
  Perturb residual gradient with noise $\boldsymbol{z}_t^{(2)} \sim \mathcal{N}\left(0, \sigma_2^2 \boldsymbol{I}_k\right)$: r_t :=sum over rows of $\hat{R}_t$, $\hat{r}_t := r_t + \boldsymbol{z}_t^{(2)}$
  $\hat{v}_t := (\hat{w}_t^\top V_k^{pub} + \hat{r}_t)/n$
  `// Update weights`
  $\boldsymbol{\theta}_{t+1} = \boldsymbol{\theta}_t - \eta \hat{v}_t$
end for

B Experiments Setting

Model Architecture. As to *pre-conditioning* experiments, for Fashion MNIST, we use a simple convolutional neural network with around 26000 parameters as in Table 5a. For SVHN and CIFAR-10, we use ResNet20 which contains roughly 260,000 parameters. Batch normalization layers are replaced by group normalization layers for different private training, aligning with GEP settings. For ChestX-ray14, we use ResNet152 which has been pretrained on ImageNet1k, a subset of the full ImageNet Deng et al. (2009) dataset. We privately fine-tune its classification layer, which contains around 28,000 parameters. We use the same model architecture for subspace distance computation and GEP private training. As to *second-phase* experiments, we evaluate ChestX-ray14, HAM10000 on ResNet152, DenseNet121, and ViT using various parameter-efficient fine-tuning techniques, we list them in Table 6. We use a simple 2-layer CNN for the probe network, shown in Table 5b.

Table 5: Self-designed model architectures.

(a) Model architecture for Fashion MNIST

Layer	Parameters
Conv2d	16 filters of 8x8, stride=2
Maxpooling2d	stride=2
Conv2d	32 filters 4x4, stride=2
Linear	32 units
Softmax	10 units

(b) Model architecture for Probe Network

Layer	Parameters
Conv2d	64 filters of 8x8, stride=5
Maxpooling2d	stride=2
Conv2d	16 filters 4x4, stride=3
Maxpooling2d	stride=2
Linear	144 units
Sigmoid	num_classes

Table 6: Parameter-efficient fine-tuning mechanisms for different models.

Model	Fine-tuning mechanism
ResNet152	fc + layer3.32.conv1.weight
DenseNet121	classifier + features.denseblock3.denselayer23.conv1.weight + features.denseblock3.denselayer24.conv1.weight
ViT	LoRA ($\alpha = 8, r = 8$)

Dataset Choice. CIFAR-10, SVHN and Fashion MNIST are commonly used for evaluation purposes in Computer Vision. For all the evaluations in Table 2, we use the first 2000 images in the test set as public images. For medical datasets, ChestX-ray14 consists of frontal view X-ray images with 14 different classes of lung disease. In our evaluation, there are 78,466 training examples and 20433 testing examples in ChestX-ray14. HAM10000 is composed of 10,000 dermatoscopic images of pigmented lesions. Our choices of public datasets for the four private datasets are described in Table 7. Among them, MNIST-M Ganin et al. (2016) consists of MNIST digits placed on randomly selected backgrounds taken from color photos in the BSDS500 dataset. FLOWER Nilsback & Zisserman (2008) consists of 102 flower categories. KagChest Kermany et al. (2018) imagees were selected from retrospective cohorts of pediatric patients of one to five years old from Guangzhou Women and Children's Medical Center, Guangzhou. It is easy to be obtained from Kaggle so we name it KagChest. SprXRay is another public chest x-ray dataset designed to help predict the age and gender of the patient based on the X-Ray image de Aguiar Kuriki et al. (2023). Kneeos is a dataset Ahmed & Mstafa (2022) that includes X-ray images of knees, which can be used for detecting knee joint issues and grading the severity of knee osteoarthritis using the Kellgren-Lawrence (KL) scale. CheXpert Irvin et al. (2019) is another chest x-ray dataset by Stanford. Similarly for the KagSkin Fanconi (2019), which images of benign skin moles and malignant skin moles. We split the first 300 (for ChestX-ray14, this number is 2000) images in the testset and take them as public. The next 300 (again, for ChestX-ray14, this number is 2000) images are the chose private examples.

Hyperparameter Setting. We use $\epsilon = 2$ and $\delta = 1e - 5$ for all the evaluations. For distance computation, we choose $k = 16$. We follow the hyperparameter setting in the GEP paper for evaluation. In the GEP paper, they didn't evaluate GEP on the ChestX-ray14 dataset. In our evaluation, we choose $k = 100$ and clip norms are 3 and 1 for original and residual gradients, respectively. The learning rate for the SGD optimizer is set to 0.05. All other hyperparameters are set as default. For second-phase pre-training, we use those public examples to perform supervised learning on trainable parameters. We use Adam optimizer and set $\eta = 3e - 3$ for Transformer-based models and $\eta = 5e - 5$ for CNN-based models. For private fine-tuning, we use SGD optimizer and set $\eta = 0.8$ and clip norm $= 0.1$.

Compute. Experiments are conducted on a Linux cloud server with one NVIDIA A100 GPU.

Table 7: Choices of public dataset for private dataset. The four datasets in the first row are private datasets. The datasets listed in the first columns are choices of public datasets. 'X' means we choose the two corresponding datasets as a pair of private/public dataset.

	CIFAR-10	SVHN	Fashion MNIST	ChestX-ray14	HAM10000
CIFAR-10	X				
CIFAR-100	X	X		X	X
SVHN	X	X			
MNIST-M		X			
Fashion MNIST			X		
FLOWER			X		
MNIST			X		
ChestX-ray14				X	
KagChest				X	X
HAM10000					X
KagSkin					X
SprXRay				X	
CheXpert				X	
Kneeos				X	

C Private Distance Measurement

While Algorithm 1 has relatively low data exposure (requiring only a single batch of private examples), it is not differentially private. In this section, we give a general algorithm that computes GSD differentially privately: Differentially Private Gradient Subspace Distance (DP-GSD, Algorithm 3). As GSD needs top-k singular vectors from private examples, we derive these singular vectors in a differentially private manner, and the rest of the algorithm remains DP because of post-processing.

Algorithm 3 Differentially Private Gradient Subspace Distance (DP-GSD)

Input: m private examples x_{priv}, m public examples x_{pub}, loss function $\mathcal{L}$, model weights $\mathbf{w}_0$, dimension k, privacy parameter ϵ, δ, clip norm c

Output: Distance between two image datasets $\boldsymbol{d}$

1: `// Compute per-sample gradient matrix for private and public examples`
2: $G_{priv} = \nabla\mathcal{L}(\mathbf{w}_0, x_{priv})$
3: $G_{pub} = \nabla\mathcal{L}(\mathbf{w}_0, x_{pub})$
4: `// Privately compute top-`k` subspace of the private gradient matrix`
5: Clip per-row: $G_{priv} = \mathbf{Clip}(G_{priv}, c)$
6: Compute $V_k^{priv} \leftarrow \mathbf{DPPCA}(G_{priv}, k, \epsilon, \delta)$
7: `// Compute top-`k` subspace of the public gradient matrix`
8: $U^{pub}, S^{pub}, V^{pub} \leftarrow \mathbf{SVD}(G_{pub})$
9: `// Compute the distance between two subspaces`
10: $\boldsymbol{d} = \mathbf{ProjectionMetric}(V_k^{priv}, V_k^{pub})$

At a high level, DP-GSD makes one adaptation to GSD: we compute top-k subspace of the private per-sample gradient matrix in a differentially private manner. **DPPCA** in line 6 of Algorithm 3 can be any Differentially Private Principal Component Analysis (DPPCA), e.g., input perturbation Chaudhuri et al. (2013), subspace perturbation Dwork et al. (2014), exponential mechanism Chaudhuri et al. (2013) and stochastic methods Liu et al. (2022).

We give a theoretical analysis of the privacy and utility guarantee of DP-GSD based on the implementation of DPPCA Chaudhuri et al. (2013), given in Algorithm 4.

Algorithm 4 Differentially Private Principal Component Analysis (DPPCA)

Input: $m \times p$ data matrix X, dimension k, privacy parameter ϵ
Output: $\hat{V}_k$: Top-k subspace of X
1: Set $A = \frac{1}{m} X^\top X$
2: Sample $\hat{V}_k = \mathbf{BMF}\left(\frac{m\epsilon}{2} A\right)$

To achieve DP, DPPCA randomly samples a k-dimensional distribution from the matrix Bingham distribution, which has the following density function:

$$f(V|A,k,p) = \frac{1}{{}_1F_1\left(\frac{1}{2}k, \frac{1}{2}p, A\right)} \exp\left(\operatorname{tr}\left(V^T A V\right)\right) \tag{5}$$

where V is the $p \times k$ subspace and ${}_1F_1\left(\frac{1}{2}k, \frac{1}{2}p, A\right)$ is a normalization factor. We use $\mathbf{BMF}(V)$ in Algorithm 4 to denote this distribution. Thus, we have the following privacy and utility guarantees (proofs in Appendix E):

Theorem C.1. ***(Privacy Guarantee)*** *Let Algorithm 4 be an implementation of* **DPPCA** *in DP-GSD, then DP-GSD is ϵ/c^2-differentially priate.*

Theorem C.2. ***(Utility Guarantee)*** *Under the assumption that $\mathcal{L}(\mathbf{w}, x)$ is 1-Lipschitz, let Algorithm 4 be an implementation of* **DPPCA** *in DP-GSD, then for $k = 1$, the distance given by DP-GSD, $\hat{d}(V_k^{priv}, V_k^{pub})$ is (ρ, η)-close to the distance given by GSD, $d(V_k^{priv}, V_k^{pub})$, if we have*

$$m > \frac{pc^2}{\epsilon\widetilde{\lambda}(1-\sqrt{1-\rho^2})}\left(4\frac{\log(1/\eta)}{p} + 2\log\frac{8\lambda_1}{\rho^2\widetilde{\lambda}}\right) \tag{6}$$

where λ_1 is the top eigenvalue, $\lambda = \lambda_1 - \lambda_2$ is the eigen-gap, $\widetilde{\lambda} = \lambda + 2|c^2 - 1|\sigma_1^2$, p is the model dimension, c is clip norm and ϵ is the privacy parameter.

D More Experiments

D.1 Membership Inference Attack: No Better Than Random Guessing

Like other hyperparameter searches, GSD should be used locally and only the best public dataset will be reported (e.g. CIFAR-100 for private CIFAR-10). To claim that this won't reveal sensitive information too much when we use a batch of private data for computing GSD, we evaluate it under membership inference attacks. We choose a well-studied membership inference attack introduced in Nasr et al. (2019) under white box setting and use Adversarial Robustness Toolbox (ART) (Nicolae et al., 2018), a Python library for ML under black box setting.

Based on the recommendations of Nasr et al. (2019), we have the following assumption one the adversary: White-box & Black-box, Stand-alone, Passive and Supervised:

- Black-box refers to the situation where the attacker can only obtain the output. White-box means the attacker can access the full model: intermediate computations, gradients, etc.
- Stand-alone means that GSD is computed in a centralized manner.
- Passive means that the attacker can observe the computation. The attacker cannot be part of the computation in the federated learning setting.
- Supervised: we assume that the attacker knows some of the examples in the private dataset. Note that this is a very strong (even unrealistic) assumption for the attacker. We did this evaluation to illustrate that even though the attacker have such knowledge, the attacker still cannot infer if a new example is in the private data selected for GSD or not.

The white-box membership inference attack, introduced by Nasr et al. (2019), makes use of the information from loss values, gradients, hidden layer activations, etc. They combine these information and supervisely train a binary classifier to tell if a particular image (x_i, y_i) is in x_{priv} or not. Without having access to the model, the black-box attack of Nicolae et al. (2018) trains a binary classifier on the images in a supervised manner.

Experiment Setting. Let's say based on the result by GSD: "CIFAR-100 is the best dataset for CIFAR-10" (see Table 2), the adversary wants to figure out if a particular image (x_i, y_i) is used in GSD computation or not (i.e. infer whether (x_i, y_i) in x_{priv}. Under white-box setting, we assume that the adversary knows the model we use, i.e. Resnet20. More importantly, we assume that the adversary has already known that n numbers of images we used in x_{priv}. Since the adversary knows that CIFAR-10 is the private dataset, we also assume that the adversary has access to all the CIFAR-10 datasets. (still, this is a strong and even unrealistic assumption for the adversary in practice) That is, the adversary has access to all the images in CIFAR-10 and knows n of them are the images we used in x_{priv}. The adversary wants to know which of the rest of them are in x_{priv}. The test set is composed of the rest of the images in x_{priv} and a same amount of images that are not in x_{priv}.

Table 8: Attack success rate of white-box membership inference attack. Note that $|x_{priv}| = 2000$.

	n=1000	n=1800
w/o GSD values		
Use gradients	50%	50%
Use hidden layer activations	50%	50%
w/ GSD values		
Use gradients	50.25%	50.31%
Use hidden layer activations	50.05%	50.06%

Evaluation results on white-box membership inference attack are given in Table 8. Since GSD computation doesn't require training the model, the model doesn't contain any information about the dataset, i.e., CIFAR-10, even when the adversary knows 1800 images in x_{priv}, still cannot infer whether a new image (x_i, y_i) is in x_{priv} or not. Observing these results, we give an even stronger assumption on the adversary: the adversary also knows the public datasets we use, i.e. CIFAR-100 and SVHN (see Table 2), and knows *exactly* which batch we are using. Based on the suggestions of Nasr et al. (2019), we add extra information as follows: the adversary uses those datasets to compute GSD, observes it T times, and adds these GSD values to the binary classifier. But still, the inference is as good as a random guess.

We also evaluate GSD under a black-box membership inference attack, provided by Nicolae et al. (2018). They train a shallow network as a binary classifier in a supervised manner. Results are given in Table 9. Starting the attack with pure images instead of extracting gradients, hidden layer activations seem to have a better attack success rate. But still, this poor attack success rate indicates that GSD can hardly cause privacy leakage.

Table 9: Attack success rate of black-box membership inference attack. Note that $|x_{priv}| = 2000$.

	n=1000	n=1800
Attack Success Rate	51.65%	52.19%

D.2 Gradients are in a Lower-dimensional Subspace.

We evaluate the empirical observation that the stochastic gradients stay in a lower-dimensional subspace during the training procedure of a deep learning model (Gur-Ari et al., 2018; Li et al., 2020), as shown in Figure 3. Results show that only a tiny fraction of singular values are enormous. At the same time, the rest are close to 0, meaning that most of the gradients lie in a lower-dimensional subspace, corresponding to the top singular vectors.

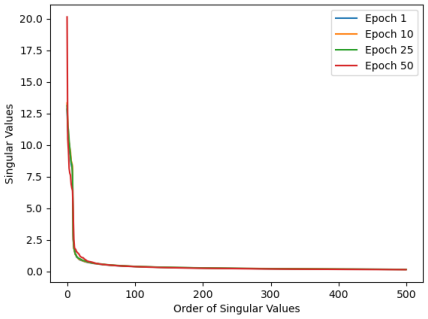

(a) CIFAR-10

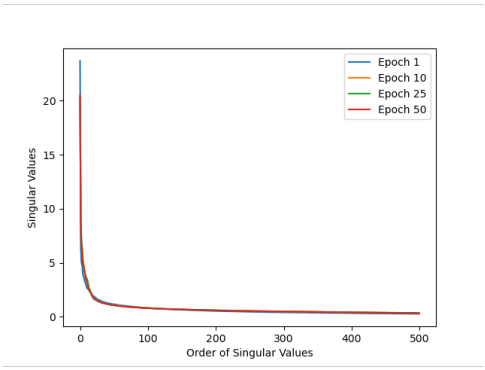

(b) ChestX-ray14

Figure 3: Top 500 singular values in the training procedure using vanilla SGD. Model architectures are in the Appendix B. Only a small fraction of singular values are extremely large while the rest are close to 0, meaning that most of the gradients lie in a lower-dimensional subspace, which corresponds to the top singular vectors.

D.3 More Pre-conditioning Evaluation.

Other than GEP, we also evaluate our method over DP Mirror Descent (Amid et al., 2022), another approach that leverages public data as a preconditioner. We give a short introduction to their algorithm in the Related Work Section 2. Following the evaluation setting in GEP, we have the following experiment results on the ChestX-ray14 dataset (Table 10).

Table 10: DP Mirror Descent evaluation AUC and corresponding distance in descending order. We use the *same* model setting for private training and distance computation. "-" means DP-SGD training without using any public data.

AUC	Private Dataset	Public Dataset	Distance
66.83%	ChestX-ray14	ChestX-ray14	**0.15**
65.79%		SprXRay	0.32
65.70%		CheXpert	0.32
64.92%		KagChest	0.36
64.76%		-	-
50.21%		CIFAR-100	0.55

The order of the public datasets is still preserved except for the fact that GEP works slightly better than DP Mirror Descent on larger datasets like ChestX-ray14.

D.4 More Second-Phase Pre-training Evaluation.

We evaluate second-phase pre-training and GSD on ChestX-ray14 and HAM10000 using ResNet152, DenseNet121, and ViT. Aside from the results we presented, we show the rest of the results here.

Table 11: Second-Phase evaluation results and corresponding distance on ChestX-ray14 in descending order. Detailed settings can be found in Appendix B. We use the ***same*** model setting for private training and distance computation. "-" means vanilla DP-SGD training.

(a) ResNet152

AUC	Private Dataset	Public Dataset	Distance
67.48%	ChestX-ray14	ChestX-ray14	**0.31**
67.27%		KagChest	0.34
66.82%		-	-
66.57%		CIFAR-100	0.39

(b) DenseNet121

AUC	Private Dataset	Public Dataset	Distance
67.53%	ChestX-ray14	ChestX-ray14	**0.33**
67.47%		-	-
67.40%		KagChest	0.37
67.28%		CIFAR-100	0.40

Table 12: Second-Phase evaluation results and corresponding distance in descending order. We use ViT and LoRA fine-tuning. We use the *same* model setting for private training and distance computation. Detailed settings can be found in Appendix B. "-" means DP-SGD training.

AUC	Private Dataset	Public Dataset	Distance
72.99%	ChestX-ray14	ChestX-ray14	**0.44**
71.86%		KagChest	0.59
70.93%		-	-
70.84%		CIFAR-100	0.98

Table 13: Second-Phase evaluation results and corresponding distance on HAM10000 in descending order. Detailed settings can be found in Appendix B. We use the ***same*** model setting for private training and distance computation. "-" means vanilla DP-SGD training.

(a) ResNet152

AUC	Private Dataset	Public Dataset	Distance
86.83%	HAM10000	HAM10000	**0.48**
85.95%		KagSkin	0.65
85.55%		-	-
85.49%		CIFAR-100	0.70
85.41%		KagChest	0.70

(b) ViT

AUC	Private Dataset	Public Dataset	Distance
84.94%	HAM10000	HAM10000	**0.50**
81.23%		KagSkin	0.76
78.65%		KagChest	0.93
77.07%		CIFAR-100	0.97
73.67%		-	-

D.5 Transferability: Simple Models Remain Predictive

GSD is transferable across different architectures and the relative GSD ordering of public datasets remains consistent. We present the results in Table 14.

Table 14: Transferability evaluation results. The left-most column denotes each pair of private-public datasets, e.g. (Xray, Xray) means we take ChestX-ray14 as a private dataset, split part of its testset and take those images as public. Detailed settings can be found in Appendix B. The first row denotes different model architectures. "Probe" is a simple CNN with around 30,000 parameters. ResNet152* and ResNet152** use different parameter-efficient fine-tuning settings. We use the same model for each Distance-Accuracy. The results show that this distance given by GSD is generally robust across different algorithms (pre-conditioning or second-phase pre-training) and different model architectures (from simple Probe to ViT). A smaller distance indicates that this public dataset is more similar to the private one, thus leveraging this public dataset for private learning will result in better accuracy.

	Probe	ResNet152*	ResNet152**	DenseNet121	ViT
Task		Pre-conditioning	Second-phase	Second-phase	Second-phase
		Distance | Accuracy			
(Xray, Xray)	**0.39**	**0.15 | 69.02%**	**0.31 | 67.48%**	**0.33 | 67.53%**	**0.44 | 72.99%**
(Xray, Chest)	0.52	0.36 | 66.62%	0.34 | 67.27%	0.37 | 67.40%	0.59 | 71.86%
(Xray, CIFAR)	0.58	0.55 | 48.80%	0.39 | 66.57%	0.40 | 67.28%	0.98 | 70.84%
(HAM, HAM)	**0.42**	-	**0.48 | 86.83%**	**0.50 | 87.06%**	**0.50 | 84.94%**
(HAM, Skin)	0.55	-	0.65 | 85.95%	0.68 | 85.53%	0.76 | 81.23%
(HAM, CIFAR)	0.67	-	0.70 | 85.49%	0.73 | 84.92%	0.97 | 77.07%
(HAM, Chest)	0.76	-	0.70 | 85.41%	0.73 | 84.88%	0.93 | 78.65%

D.6 OTDD: Generally Good But Hard to Make DP

We compare GSD with the Optimal Transport Dataset Distance (OTDD) algorithm Alvarez-Melis & Fusi (2020), which also measures dataset similarity. OTDD considers labels (Y) as distributions over features (X) and calculates the earth mover distance (Wasserstein distance) between these distributions for a dataset $D = (X, Y)$. Evaluation results can be found in Table 15.

Table 15: Results for GSD vs. OTDD. We evaluate ChestX-ray14 using GEP and compute the distance using OTDD and GSD.

	AUC	OTDD	GSD
ChestX-ray14	69.02%	64057	0.15
SprXRay	67.22%	168755	0.32
CheXpert	67.20%	135292	0.32
KagChest	66.61%	152930	0.36
Kneeos	65.37%	217431	0.38
-	64.76%	-	-
CIFAR-100	48.60%	277655	0.55

OTDD accurately orders the majority of datasets, but it struggles with "semantically close" datasets like SprXRay, CheXpert, and KagChest. This is generally not a good sign because in real-world scenarios, in-distribution public datasets are often not accessible, making it crucial to order public datasets precisely. Furthermore, while GSD is not DP itself, OTDD needs multiple direct interactions with input images, making achieving DP significantly more challenging.

D.7 More vs. Task2Vec.

We evaluate the similarity between each public-private dataset pair using Task2Vec. The results on HAM10000 public dataset are presented here using cluster map in Figure 4. The closest datasets are itself, and the HAM10000 public dataset. However, following this, the closest dataset is KagChest, which is qualitatively very different from HAM10000 (chest x-rays versus skin lesions) and provides low utility when used as the public dataset (see Table 14). In particular, KagSkin (another skin disease dataset) is qualitatively closer to HAM10000 and provides higher utility when used as a public dataset, yet Task2Vec assigns it a greater distance than KagChest. In contrast, GSD orders the quality of these datasets in a manner consistent with their quality.

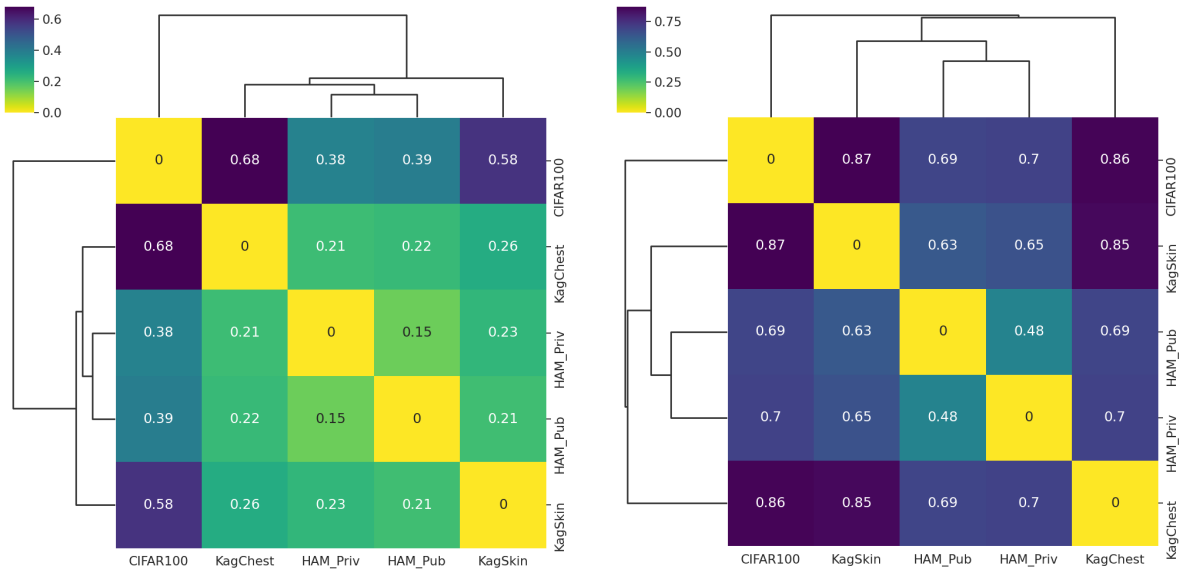

(a) Clustermap given by Task2Vec

(b) Clustermap given by GSD

Figure 4: Clustermaps given by Task2Vec (left) and GSD(right) for HAM10000 and corresponding public datasets. The lines on the top and the left denote the similarity of a pair of datasets. The numbers in the grid are the similarity distance for a pair of datasets. Although Task2Vec gives the correct prediction for (HAM_{public}, $\text{HAM}_{private}$) pair, it ***incorrectly*** predicts the second-close similarity, where it believes KagChest is the second-close dataset for HAM10000, while they should be totally irrelevant.

D.8 Combinations of Datasets Better Than One: Generally But Not Necessarily True

While some studies point out that pre-training on multiple diverse datasets can lead to better performance on downstream NLP tasks compared to pre-training on a single dataset (Brown et al., 2020), our experiment results show that under small amount of accessible public data assumption, this conclusion is generally but not necessarily true, as shown in Table 16.

Using SprXRay or CheXpert as public datasets for private learning can result in higher accuracy compared to the DP-SGD baseline. Combining these datasets can further improve accuracy. However, if a "bad" public dataset like CIFAR-100 is combined with ChestX-ray14, it can negatively impact the overall performance.

Table 16: GEP evaluation AUC and corresponding distance in descending order. We use the *same* model setting for private training and distance computation. "-" means DP-SGD training without using any public data.

AUC	Private Dataset	Public Dataset	Distance
69.02%	ChestX-ray14	ChestX-ray14	**0.15**
67.83%		SprXRay + CheXpert	0.30
67.31%		SprXRay	0.32
67.29%		CheXpert	0.32
67.12%		CheXpert + CIFAR-100	0.33
66.62%		KagChest	0.36
65.26%		Kneeos	0.38
64.90%		-	-
48.80%		CIFAR-100	0.55

E Missing Proofs

In this section, we present proofs for Section 4.1.

Lemma 4.1 (Reconstruction Error). For GEP, let $\mathbf{G}_{priv}$, V^{pub}, V^{priv} be the gradient matrix and top-1 gradient subspace from public or private examples at step t, respectively. Then we have the spectral norm of reconstruction error

$$\|\mathbf{R}\|_2 \leq \sqrt{2} s_{1,t} \mathbf{GSD}(V^{priv}, V^{pub}) + s_{k+1,t} \tag{7}$$

where $\mathbf{R} = \mathbf{G}_{priv} - \mathbf{G}_{priv} V^{pub} V^{pub\top}$ is the reconstruction error of private gradient matrix $\mathbf{G}_{priv}$ using public examples, $s_{1,t} \geq ... \geq s_{k,t} \geq ...$ are the singular values of $\mathbf{G}_{priv}$, $\mathbf{GSD}(V^{priv}, V^{pub})$ is the gradient subspace distance given by our algorithm.

Proof. We have

$$\begin{aligned} \mathbf{R} &= \mathbf{G}_{priv} - \mathbf{G}_{priv}\Pi_k^{pub} \\ &= \mathbf{G}_{priv} - \mathbf{G}_{priv}\Pi_k^{priv} + \mathbf{G}_{priv}\Pi_k^{priv} - \mathbf{G}_{priv}\Pi_k^{pub} \end{aligned} \tag{8}$$

$$\Rightarrow \quad \|\mathbf{R}\|_2 - \left\|\mathbf{G}_{priv}(\Pi_k^{pub} - \Pi_k^{priv})\right\|_2 \leq \left\|\mathbf{G}_{priv}\left(\mathbb{I} - \Pi_k^{priv}\right)\right\|_2 \tag{9}$$

$$\Rightarrow \quad \|\mathbf{R}\|_2 \leq \underbrace{\left\|\mathbf{G}_{priv}(\Pi_k^{pub} - \Pi_k^{priv})\right\|_2}_{D_1} + \underbrace{\left\|\mathbf{G}_{priv}\left(\mathbb{I} - \Pi_k^{priv}\right)\right\|_2}_{D_2} \tag{10}$$

where $\Pi_k^{pub} = V_k^{pub} V_k^{pub\top}$ denotes the orthogal projection to the subspace of $\text{span}(V_k^{pub})$, $\Pi_k^{priv} = V_k^{priv} V_k^{priv\top}$ denotes the orthogal projection to the subspace of $\text{span}(V_k^{priv})$.

For D_2, recall that the Eckart–Young–Mirsky theorem (Eckart & Young, 1936) shows that the best rank-k approximation of $\mathbf{G}_{priv}$ is given by its top-k reconstruction using SVD. Therefore, we have

$$\begin{aligned} D_2 &= \left\|\mathbf{G}_{priv}\left(\mathbb{I} - \Pi_k^{priv}\right)\right\|_2 \\ &= \left\|\sum_{i=1}^{p} s_i u_i v_i^\top - \sum_{i=1}^{k} s_i u_i v_i^\top\right\|_2 \\ &= \left\|\sum_{i=k+1}^{p} s_i u_i v_i^\top\right\|_2 \\ &= s_{k+1} \end{aligned} \tag{11}$$

For D_1, the definition of projection metric (Definition 3) shows that

$$\begin{aligned}\mathbf{GSD}^2(V_k^{priv}, V_k^{pub}) &= k - (\cos^2\theta_1 + ... + \cos^2\theta_k) \\ &\overset{(a)}{=} k - \mathrm{Tr}\left(V_k^{priv\top} V_k^{priv} V_k^{pub\top} V_k^{pub}\right) \\ &\overset{(b)}{=} \frac{1}{2}\left\|\Pi_k^{pub} - \Pi_k^{priv}\right\|_F^2\end{aligned} \tag{12}$$

(a) and (b) hold according to Equation 5.4 of Conway et al. (2002).

Therefore, we have

$$\begin{aligned}D_1 &= \left\|\mathbf{G}_{priv}(\Pi_k^{pub} - \Pi_k^{priv})\right\|_2 \\ &\leq \|\mathbf{G}_{priv}\|_2 \left\|\Pi_k^{pub} - \Pi_k^{priv}\right\|_2 \\ &\leq s_1 \left\|\Pi_k^{pub} - \Pi_k^{priv}\right\|_F \\ &= \sqrt{2} s_1 \mathbf{GSD}(V_k^{priv}, V_k^{pub})\end{aligned} \tag{13}$$

Combining D_1 and D_2, we have

$$\begin{aligned}\|\mathbf{R}\|_2 &\leq \left\|\mathbf{G}_{priv}(\Pi_k^{pub} - \Pi_k^{priv})\right\|_2 + \left\|\mathbf{G}_{priv}\left(\mathbb{I} - \Pi_k^{priv}\right)\right\|_2 \\ &\leq \sqrt{2} s_{1,t} \mathbf{GSD}(V_k^{priv}, V_k^{pub}) + s_{k+1,t}\end{aligned} \tag{14}$$

Setting $k = 1$ yields a tighter bound as $\left\|\Pi_k^{pub} - \Pi_k^{priv}\right\|_2 = \left\|\Pi_k^{pub} - \Pi_k^{priv}\right\|_F$. Thus we know that GSD bounds the reconstruction error at step t. □

Theorem 4.2 (Excess Risk). Assume that the loss $L(\mathbf{w}) = \frac{1}{n}\sum_{i=1}^n \ell(\mathbf{w}, z_i)$ is 1-Lipschitz, convex, and β-smooth. Let $\mathbf{w}^* = \mathrm{argmin}_{w\in\mathcal{W}} L(\mathbf{w})$. The excess risk of GEP obeys

$$\mathbb{E}[L(\overline{\mathbf{w}})] - L(\mathbf{w}^*) \leq O\left(\frac{\sqrt{k\log(1/\delta)}}{n\epsilon}\right) + O\left(\frac{\sqrt{p\log(1/\delta)}}{n\epsilon}\overline{\mathbf{d}}\right) \tag{15}$$

where GEP is (ϵ, δ)-DP (see Appendix A). Here we set $\eta = \frac{1}{\beta}, T = \frac{n\beta\epsilon}{\sqrt{p}}$, $\overline{\mathbf{w}} = \frac{1}{T}\sum_{t=1}^T \mathbf{w}_t$, $\overline{\mathbf{d}} = \frac{1}{T}\sum_{t=1}^T d_t^2$, $d_t = \sqrt{2} s_{1,t}\mathbf{GSD} + s_{k+1,t}$, **GSD** is the gradient subspace distance when setting subspace dimension to 1, and s_t are singular values of the gradient matrix at step t.

Proof. Theorem 3.3 of Yu et al. (2021) (see Appendix A) shows that the excess risk of GEP obeys

$$\mathbb{E}[L(\overline{\mathbf{w}})] - L(\mathbf{w}^*) \leq O\left(\frac{\sqrt{k\log(1/\delta)}}{n\epsilon}\right) + O\left(\frac{\overline{r}\sqrt{p\log(1/\delta)}}{n\epsilon}\right) \tag{16}$$

where $\overline{r} = \frac{1}{T}\sum_{t=0}^{T-1} r_t^2$ and $r_t = \|\mathbf{G}_{priv} - \mathbf{G}_{priv} V_k^{pub} V_k^{pub\top}\|_2$ is the reconstruction error at step t.

From Lemma 4.1 we know that $r_t \leq d_t$ at each step t, for any $k \geq 1$, thus completing the proof. □

Lemma E.1. ***(Theorem 6 of Chaudhuri et al. (2013))*** *DPPCA (Algorthim 4) is ϵ-differentially private.*

Theorem C.1 (Privacy Guarentee). Let Algorithm 4 be an implementation of **DPPCA** in DP-GSD, then DP-GSD is ϵ/c^2-differentially priate.

Proof. Let x_{priv} be m private examples. $G_{priv} = \mathbf{Clip}(\nabla\mathcal{L}(\mathbf{w}_0, x_{priv}), c) \in \mathbb{R}^{m\times p}$ is per-sample gradient matrix and $A = \frac{1}{m}G_{priv}G_{priv}^\top$. We sample top-$k$ eigenvectors from the matrix Bingham distribution (Chikuse, 2003):

$$f(V|A,k,p) = \frac{1}{{}_1F_1\left(\frac{1}{2}k, \frac{1}{2}p, A\right)} \exp\left(\operatorname{tr}\left(V^T A V\right)\right) \tag{17}$$

with $A = \frac{m\epsilon}{2c^2}A$. We show that this is the exponential mechanism applied to the score function $q(V;x) = mv^TAv$.

Consider the neighboring data $X'_{priv} = [x_1, ..., x'_i, ..., x_m]$ that differ from X_{priv} with one data example x'_i. Let $G'_{priv} = \mathbf{Clip}(\nabla\mathcal{L}(\mathbf{w}_0, x'_{priv}), c)$ and $A' = \frac{1}{m}G'^\top_{priv}G'_{priv}$. We have

$$\begin{aligned}\Delta q = \max\left|mv^TAv - mv^TA'v\right| &\leq \left|v^T(g_ig_i^T - g'_ig_i'^\top)v\right| \\ &\leq \left|\|v^Tg_i|\|^2 - \|v^Tg'_i\|^2\right| \\ &\leq \left|\|v^T\nabla\mathcal{L}(\mathbf{w}_0, x_i)|\|^2 - \|v^T\nabla\mathcal{L}(\mathbf{w}_0, x'_i)\|^2\right| \\ &\leq c^2\end{aligned} \tag{18}$$

Therefore, from E.1, we know that **DPPCA** in DP-GSD (Algorithm 3) is ϵ/c^2-differentially private. Thus, DP-GSD is ϵ/c^2-differentially private because of post-processing. □

Lemma E.2. ***(Theorem 7 of Chaudhuri et al. (2013))*** *Let $k = 1$, the private gradient subspace V_k^{priv} in GSD and the private gradient subspace $\hat{V}_k^{priv}$ from Algorithm 4 satisfy*

$$\Pr\left(\left|\left\langle V_k^{priv}, \hat{V}_k^{priv}\right\rangle\right| > \rho\right) \geq 1 - \eta \tag{19}$$

if we have

$$m > \frac{p}{\epsilon\alpha(1-\rho)}\left(4\frac{\log(1/\eta)}{p} + 2\log\frac{8\lambda_1}{(1-\rho^2)\,\alpha}\right) \tag{20}$$

where λ_1 is the top eigenvalue, $\alpha = \lambda_1 - \lambda_2$ is the eigen-gap, p is the model dimension and ϵ is the privacy parameter.

Theorem C.2 (Utility Guarantee) Under the assumption that $\mathcal{L}(\mathbf{w}, x)$ is 1-Lipschitz, let Algorithm 4 be an implementation of **DPPCA** in DP-GSD, then for $k = 1$, the distance given by DP-GSD, $\hat{d}(V_k^{priv}, V_k^{pub})$ is (ρ, η)-close to the distance given by GSD, $d(V_k^{priv}, V_k^{pub})$, if we have

$$m > \frac{pc^2}{\epsilon\widetilde{\lambda}(1-\sqrt{1-\rho^2})}\left(4\frac{\log(1/\eta)}{p} + 2\log\frac{8\lambda_1}{\rho^2\widetilde{\lambda}}\right) \tag{21}$$

where λ_1 is the top eigenvalue, $\lambda = \lambda_1 - \lambda_2$ is the eigen-gap, $\widetilde{\lambda} = \lambda + 2|c^2 - 1|\sigma_1^2$, p is the model dimension, c is clip norm and ϵ is the privacy parameter.

Proof. Let x be m examples, $\boldsymbol{G} = \nabla\mathcal{L}(\mathbf{w}_0, x) \in \mathbb{R}^{m\times p}$ be the corresponding gradients, $\tilde{\boldsymbol{G}} = \texttt{Clip}(\boldsymbol{G}, c)$, $\boldsymbol{A} = \boldsymbol{G}^\top\boldsymbol{G}$, $\widetilde{\boldsymbol{A}} = \tilde{\boldsymbol{G}}^\top\tilde{\boldsymbol{G}}$, $\Delta\boldsymbol{A} = \boldsymbol{A} - \widetilde{\boldsymbol{A}}$. Let $\lambda = \lambda_1(\boldsymbol{A}) - \lambda_2(\boldsymbol{A})$ be the eigen gap of $\boldsymbol{A}$, $\widetilde{\lambda} = \lambda_1(\widetilde{\boldsymbol{A}}) - \lambda_2(\widetilde{\boldsymbol{A}})$ be the eigen gap of $\boldsymbol{A}$. Applying Wely's inequality, we have:

$$\left|\lambda_1(\widetilde{\boldsymbol{A}}) - \lambda_1(\boldsymbol{A})\right| \leq \|\Delta\boldsymbol{A}\|, \quad \left|\lambda_2(\widetilde{\boldsymbol{A}}) - \lambda_2(\boldsymbol{A})\right| \leq \|\Delta\boldsymbol{A}\| \tag{22}$$

Thus, we have:

$$\widetilde{\lambda} \leq \lambda + 2||\Delta \boldsymbol{A}|| \tag{23}$$

Assume that every gradient will be clipped, let $\boldsymbol{D}$ be a diagonal matrix with diagonal entries $D_{ii} = \frac{c}{||\boldsymbol{g}_i||_2}$ where $\boldsymbol{g}_i, i = 1, \ldots, m$ is the row of $\boldsymbol{G}$. Therefore, $\widetilde{\boldsymbol{A}} = \boldsymbol{G}^\top \boldsymbol{D}^2 \boldsymbol{G}$, and

$$\begin{aligned} \|\Delta \boldsymbol{A}\| &= \|\widetilde{\boldsymbol{A}} - \boldsymbol{A}\| = \|\boldsymbol{G}^\top \boldsymbol{D}^2 \boldsymbol{G} - \boldsymbol{G}^\top \boldsymbol{G}\| \\ &= \|\boldsymbol{G}^\top (\boldsymbol{D}^2 - \boldsymbol{I}) \boldsymbol{G}\| \\ &\leq |c^2 - 1| \|\boldsymbol{G}^\top \boldsymbol{G}\| \\ &= |c^2 - 1| \sigma_1^2 \end{aligned} \tag{24}$$

where σ_1 is the largest singular value of $\boldsymbol{G}$. Therefore we have

$$\begin{aligned} \widetilde{\lambda} &\leq \lambda + 2||\Delta \boldsymbol{A}|| \\ &\leq \lambda + 2|c^2 - 1|\sigma_1^2 \end{aligned} \tag{25}$$

Let V_k^{priv} be the private gradient subspace in GSD and $\hat{V}_k^{priv}$ be the private gradient subspace in DP-GSD, $d(V_k^{priv}, \hat{V}_k^{priv})$ be the projection metric distance between two subspaces. From Lemma E.2, we have

$$\begin{aligned} &\Pr\left(\left|\left\langle V_k^{priv}, \hat{V}_k^{priv} \right\rangle\right| > \mu\right) = \Pr\left(d(V_k^{priv}, \hat{V}_k^{priv}) \leq \sqrt{1-\rho^2}\right) \geq 1 - \eta \\ &\xrightarrow{(a)} \Pr\left(\left|\hat{d}(V_k^{priv}, V_k^{pub}) - d(V_k^{priv}, V_k^{pub})\right| \leq \sqrt{1-\mu^2}\right) \geq 1 - \eta \end{aligned} \tag{26}$$

(a) holds because of the triangle inequality of projection metric (Ham & Lee, 2008). Substituting $\sqrt{1-\mu^2}$ with ρ, and λ with $\widetilde{\lambda}$ in Lemma E.2, we have $\hat{d}(V_k^{priv}, V_k^{pub})$ is (ρ, η)-close to $d(V_k^{priv}, V_k^{pub})$. □